Liposome-loaded polymeric microneedles for enhanced skin deposition of rifampicin

Document Version:
Publisher's PDF, also known as Version of record

Queen's University Belfast - Research Portal:
Link to publication record in Queen's University Belfast Research Portal

Liposome-loaded polymeric microneedles for enhanced skin deposition of rifampicin

Qonita Kurnia Anjani [a,b], Anjali K. Pandya [a,c], Sara Demartis [d], Juan Domínguez-Robles [a,e], Natalia Moreno-Castellanos [f], Huanhuan Li [a], Elisabetta Gavini [g], Vandana B. Patravale [c], Ryan F. Donnelly [a,*]

[a] School of Pharmacy, Queen's University Belfast, Medical Biology Centre, 97 Lisburn Road, Belfast BT9 7BL, UK
[b] Fakultas Farmasi, Universitas Megarezky, Jl. Antang Raya No. 43, Makassar 90234, Indonesia
[c] Department of Pharmaceutical Sciences and Technology, Institute of Chemical Technology, Nathalal Parekh Marg, Matunga, Mumbai, Maharashtra 400 019, India
[d] Department of Chemical, Physical, Mathematical and Natural Sciences, University of Sassari, Piazza Università 21, 07100 Sassari, Italy
[e] Department of Pharmacy and Pharmaceutical Technology, Faculty of Pharmacy, Universidad de Sevilla, 41012 Seville, Spain
[f] Basic Science Department, Faculty of Health, Universidad Industrial de Santander, Bucaramanga 680001, Colombia
[g] Department of Medicine, Surgery and Pharmacy, University of Sassari, Piazza Università 21, Sassari 07100, Italy

ABSTRACT

Methicillin-resistant *Staphylococcus aureus* (MRSA) is a prevailing bacterial pathogen linked to superficial skin and soft tissue infections (SSTIs). Rifampicin (RIF), a potent antibiotic against systemic and localised staphylococcal infections, faces limitations due to its low solubility. This constraint hampers its therapeutic potential for MRSA-induced SSTIs. To address this, an advanced liposomal system was designed for efficient dermal RIF delivery. Rifampicin-loaded liposomes (LipoRIF) were embedded within polymeric dissolving microneedles (DMNs) to enable targeted intradermal drug delivery. A robust Design of Experiment (DoE) methodology guided the systematic preparation and optimisation of LipoRIF formulations. The optimal LipoRIF formulation integrated within polymeric DMNs. These LipoRIF-DMNs exhibited favourable mechanical properties and effective skin insertion characteristics. Notably, *in vitro* assays on skin deposition unveiled a transformative result – the DMN platform significantly enhanced LipoRIF deposition within the skin, surpassing LipoRIF dispersion alone. Moreover, LipoRIF-DMNs displayed minimal cytotoxicity toward cells. Encouragingly, rigorous *in vitro* antimicrobial evaluations demonstrated LipoRIF-DMNs' capacity to inhibit MRSA growth compared to the control group. LipoRIF-DMNs propose a potentially enhanced, minimally invasive approach to effectively manage SSTIs and superficial skin ailments stemming from MRSA infections.

1. Introduction

Staphylococcus aureus (S. aureus) is a Gram-positive bacterium responsible for heterogeneous diseases ranging from superficial skin and soft tissue infections (SSTIs) to endocarditis. Uncomplicated SSTIs include minor infections (cellulitis, folliculitis, furunculosis, etc.). However, complicated SSTIs, such as necrotising fasciitis, involve deeper tissues and a mortality rate higher than 30 % is observed in the case of systemic invasion (Nandhini et al., 2022; Giacobbe et al., 2022). In recent decades, SSTIs have seen increased complications and recurrences, with a parallel intensification of hospitalisations (Kaye et al.,

2019; Suaya et al., 2013). In this regard, methicillin-resistant *S. aureus* (MRSA) is the predominant cause (Nandhini et al., 2022) as it may represent 46 % of *S. aureus* invading SSTIs patients, which in turn represent 81 % of pathogen-positive specimens (Hindy et al., 2022). MRSA multi-drug resistance (MDR) is well-known; also, it rapidly spreads, resulting in one of the primary reasons for community-acquired infections, which brings about critical consequences beyond the massive impact on healthcare costs (Giacobbe et al., 2022). According to the World Health Organization (WHO), delineating safe and effective protocols to prevent and control MRSA infections is one of the critical clinical challenges worldwide (Zasowski et al., 2022).

* Corresponding author at: Chair in Pharmaceutical Technology, School of Pharmacy, Queen's University Belfast, Medical Biology Centre, 97 Lisburn Road, Belfast BT9 7BL, Northern Ireland, UK.
E-mail address: r.donnelly@qub.ac.uk (R.F. Donnelly).

Rifampicin (RIF) is a macrocyclic antibiotic highly effective against systemic and local staphylococcal infections, since it penetrates biofilms and kills organisms in the sessile growth phase (Zheng and Stewart, 2002). Notably, RIF proved active against *S. aureus* and MRSA (Forrest and Tamura, 2010; Zimmerli and Sendi, 2019; Perlroth et al., 2008). Still, RIF use as monotherapy has been abandoned due to the rapid rise of resistance. While combination therapy has been reported to eradicate *S. aureus*-induced SSTIs, its application to clinical practice is not frequent (Perlroth et al., 2008). RIF is mainly administered orally at 600 mg daily on an empty stomach because its absorption is halved by food (Pcloquin et al., 1999). Undesirable consequences of RIF administration may include queasiness, loss of appetite, bowel issues, skin redness or irritation, and inadequate functioning of the adrenal gland. In addition, it may lead to temporary and symptomless increases in the levels of certain liver enzymes and bilirubin in the bloodstream (Rifampicin, n. d.). Furthermore, RIF induces various enzymes involved in drug metabolism and it may reduce the effect of several pharmacological classes, including anticoagulants, benzodiazepines, corticosteroids and hormonal contraceptives. In this regard, the concurrent administration of RIF with isoniazid or some antiretrovirals must be avoided, since it increases the risk of severe hepatotoxicity (Zimmerli and Sendi, 2019; Perlroth et al., 2008; Singh et al., 2014). Even though it is a long-standing drug with a challenging profile, RIF could still have a relevant impact on eradicating SSTIs. However, the therapeutic potential must be maximised to relaunch this clinical use. To reach this aim, drug delivery science plays a pivotal role.

Nanotechnology-based therapeutics, often referred to as 'nano-drugs', have proven effective in combating MDR species. These approaches enhance drug accumulation at the target site by facilitating cellular uptake and subsequent controlled release, which can enhance the pharmacological impact (Makabenta et al., 2020; Malaekeh-Nikouei et al., 2020; Hulme, 2022; Obinu et al., 2020). Nano-antibiotics may evade existing resistance mechanisms and may be less prone to induce resistance than conventional antibiotics. In addition, nano-antibiotics act as distractions, reducing the impact of virulent microbial factors on indigenous microflora, which is essential to maintain proper tissue function (Hulme, 2022). This point is an evident concern in the co-morbidity of SSTIs and other skin diseases. For example, colonisation by MRSA is recurrent in patients suffering from atopic dermatitis, augmenting the skin microbial dysbiosis, allergen sensitisation, development of the atopic march, and food allergy (Kim et al., 2023). Thus, nano-antibiotic-based treatment could apport several benefits to SSTI patients. In the vast arena of nanodrugs, the increasing prevalence of MRSA has increased the investigations on liposomal antibiotics to promote the clearance of the pathogen while contributing to skin function regeneration. This is due to their biocompatibility, biodegradability, improved drug stability, low toxicity and lack of immune system activation (Gonzalez Gomez and Hosseinidoust, 2020; Ferreira et al., 2021). Remarkably, liposomes enhance antibiotic interactions with the bacterial lipid membranes through four mechanisms: (i) fusion with the membrane, (ii) adsorption through electrostatic force, (iii) lipid exchange and (iv) endocytosis. Thus, antibiotic delivery would be targeted and the therapeutic dose would be decreased, reducing adverse effects (Gonzalez Gomez and Hosseinidoust, 2020). In this regard, liposomes applied topically to the skin have been proposed as a way to directly target MRSA colonies. This method offers several advantages over the conventional oral route, including the ability to avoid or minimize antibiotic absorption into the bloodstream, which reduces its spread to non-infected organs (Hulme, 2022; El-Naggar et al., 2023; Rukavina et al., 2018). Moreover, skin delivery would bypass the pre-systemic first-pass metabolism responsible for drug interactions (Wiedersberg and Guy, 2014). Nevertheless, the central limit of liposomes is represented by the high percentage of ruptures and drug leakage in the outmost skin layers due to their rigid structure. Thus, the intact vesicle may not be able to reach the infected site and the advantageous interaction between liposome and cells would be lost (Oyarzún et al., 2021;

Demartis et al., 2021). Modifications to conventional liposomes have been performed to obtain highly flexible vesicles able to migrate intact through the skin layers; still, their application is beneficial when systemic absorption is desired (Opatha et al., 2020; Cevc, 1996). Thus, other strategies must be considered to ensure the local deposition of liposomal antibiotics.

Microneedle array patches (MNs) represent a painless and self-administrable microinjection device consisting of a multitude of micron-sized needles (25–1500 μm) which, upon application to the skin surface, pierce the *stratum corneum* (SC) and create reversible micro-channels that enable deposition of the active cargo directly in the skin layers (Coulman et al., 2009; Sabri et al., 2020). Different types of MNs are reported in the literature. However, in recent years, there has been a substantial growing interest in polymer-based dissolving MNs (DMNs) (Sartawi et al., 2022; Salwa et al., 2021). DMNs are fabricated with hydrosoluble, biodegradable, or biocompatible polymers, which dissolve in the tissue fluid and release the nanodrug in a controlled manner with exact drug dosage. The characteristics of being biocompatible avoids the need for post-treatment removal and pose minimal risk of inflammation or infection (Guillot et al., 2020). Notably, recent works have highlighted the success of including liposomes in DMNs to provide dermal delivery (Demartis et al., 2022; Huang et al., 2022; Peng et al., 2021) and the benefits of coupling antibiotics with MNs techniques to treat skin infections (Jamaledin et al., 2020; Anjani et al., 2022; Permana et al., 2020; Anjani et al., 2023).

This study aims to develop and characterise DMNs capable of loading LipoRIF, a liposomal formulation of RIF. This innovative approach is designed to address MRSA-induced SSTIs and tackle multidrug resistance. DMNs were selected to ensure a controlled dosage and intradermal release of LipoRIF. To reach this goal, Lipo-RIF dispersions were prepared and optimised by Design of Experiments (DoE) methods and subsequently tested for liposome characterisation. In the second step, LipoRIF dispersion was freeze-dried and loaded into DMNs for the final formulation (LipoRIF-DMNs). LipoRIF-DMNs were evaluated for their *in vitro* and *ex vivo* physicochemical and mechanical properties, biocompatibility and antimicrobial activity. The structural integrity of LipoRIF following loading into LipoRIF-DMNs was investigated. Finally, an *ex vivo* dermatokinetic study was performed on excised neonatal porcine skin to determine the intradermal delivery efficiency of the novel RIF delivery system.

2. Materials and methods

2.1. Materials

Rifampicin (RIF) (purity > 98 %) was procured from Tokyo Chemical Industry (Oxford, UK). The phospholipid used for liposome preparation, Lipoid S 100® – Soybean phosphatidylcholine, was a kind gift from Lipoid GmbH (Ludwigshafen, Germany). Poly(vinyl alcohol) (PVA, MW 10,000 g/mol) and poly(vinylpyrrolidone) were procured from Sigma-Aldrich (Dorset, UK). Plasdone™ K-29/32 (PVP, MW 58,000 g/mol) and Plasdone™ K-90 (PVP, MW 1,300,000 g/mol) were purchased from Ashland Industries Europe GmbH (Schaffhausen, Switzerland). Glycerol was purchased from VWR (Leicestershire, UK). Phosphate-buffered saline tablets (PBS, pH 7.3–7.5) were purchased from Sigma-Aldrich (Dorset, UK). All the solvents employed were of analytical grade and purchased from Sigma-Aldrich (Dorset, UK).

2.2. High-performance liquid chromatography (HPLC) analysis

The quantity of RIF was measured using high-performance liquid chromatography (HPLC) (Agilent Technologies 1220 Infinity UK Ltd., Stockport, UK) by following the same method as adapted from previous research (Anjani et al., 2021; Anjani et al., 2021). The samples were analysed using a Phenomenex® Luna C18 (ODS1) column (150 × 4.6 mm internal diameter, 5 μm packing). The sample analysis was carried

out at a flow rate of 1 mL/min with an injection volume of 50 μL. The mobile phase was made up of a mixture of 25 mM sodium dihydrogen phosphate buffer (with 1 % triethylamine and adjusted using phosphoric acid to pH 6.8) as an aqueous phase (A) and methanol (B) as an organic phase with a ratio of (30A:70B, %v/v). The samples were detected at a UV wavelength of 334 nm. The Agilent ChemStation® Software B.02.01 was used to analyse all chromatograms.

2.3. Formulation and characterisation of LipoRIF dispersion

2.3.1. Preparation and optimisation of LipoRIF dispersion

LipoRIF dispersion was obtained by a solvent injection method (Wagner and Vorauer-Uhl, 2011). Briefly, the organic phase was prepared by dissolving Lipoid S 100® and RIF in a mix of methanol and chloroform (1:1 ratio) using a vortex at 2,500 rpm for 30 sec at room temperature (r.t.). The organic phase was then injected into the 5 mL of aqueous phase (PBS pH 7.4) using a 1 mL syringe with 26G needles (0.45 × 13 mm) under continuous magnetic stirring. The resulting mixture was kept under magnetic stirring uncovered overnight to ensure complete solvent evaporation and obtain the LipoRIF. The DoE approach (Design-Expert, StatEase®, Minneapolis, MN, USA) was employed to optimise LipoRIF dispersion predicting the most suitable formulation and process parameters. Evaluated parameters were RIF to lipid ratio, organic phase volume and stirring rate of organic and aqueous phases. Unloaded formulation (ULipo) was prepared as a comparison.

2.3.2. Dimensional profile

The NanoBrook Omni™ particle sizer and zeta potential analyzer (Brookhaven NY, USA) was used to assess the particle size, polydispersity index (PDI), and zeta potential of LipoRIF and ULipo dispersions. The measurements were conducted in triplicate. Dynamic light scattering (DLS) was employed to determine the particle size and PDI. Samples were diluted (1:100 dilution) with ultrapure water to ensure that their concentration was within the instrument's required range. The analyses were performed under the following conditions: fluid refractive index of 1.333; temperature of 25 °C; viscosity of 0.890 cP; scattering angle of 90°; equilibration time of 3.0 min; and a sample run time of 300 s.

2.3.3. Drug loading and entrapment efficiency

The drug loading and entrapment efficiency of RIF in LipoRIF suspension were determined quantitatively. The analyses were conducted in triplicate. To determine drug loading, 0.1 mL of LipoRIF dispersion was dissolved in 1.9 mL of methanol using an Eppendorf ThermoMixer® (Eppendorf Ltd, Stevenage, UK) at room temperature with a speed of 1,500 rpm for 15 mins. The resulting solution was subjected to a validated HPLC method described in Section 2.2. The drug loading (DL) was calculated using Equation (1):

$$DL(\%) = \frac{Total \ RIF \ quantified}{Theoretical \ RIF \ used} \times 100 \qquad (1)$$

To determine the entrapment efficiency (EE), 0.5 mL of LipoRIF dispersion was first centrifuged at 15,300 rpm at 4 °C for 30 mins using Amicon Ultra – 0.5 mL centrifugal filters (Ultracel – 10 K, Merck Millipore Ltd., Cork, Ireland) to separate LipoRIF from the unentrapped drug. Then, the unentrapped drug was quantified by HPLC, and EE was calculated as in Equation (2):

$$EE(\%) = \frac{Total \ RIF \ quantified - free \ RIF}{Total \ RIF \ quantified} \times 100 \qquad (2)$$

2.3.4. Transmission electron microscopy

The morphology of LipoRIF and unloaded liposome (ULipo) dispersions was examined using a transmission electron microscope (TEM), specifically the JEOL JEM 1400-plus transmission electron microscope (JEOL UK, Welwyn Garden City, UK) with an accelerating voltage of

120 kV. To conduct the analysis, droplets of diluted sample of both ULipo and RIF-LIP dispersions were deposited onto a Formvar film-coated copper grid (Agar Scientific Ltd, Essex, UK) and stained with uranyl acetate. The grids were washed with deionized water and left to dry for 2 h at room temperature before being analysed.

2.3.5. Stability studies

The storage stability of LipoRIF dispersion was evaluated in terms of drug loading, particle size and PDI over time after storing samples at 25 °C/RH 65 %. Samples were analysed at each predetermined time (7, 14, 30, 60 and 90 days). Dimensional profile and drug loading were determined, as reported in sections 2.2.2 and 2.2.3. The stability of RIF under accelerated conditions was also evaluated; in this case, LipoRIF were stored at 40 °C/RH 75 % and analysed at 30 days.

2.3.6. In vitro release study

In order to investigate the release pattern of RIF from LipoRIF dispersion, a dialysis bag experiment was conducted (Faizi et al., 2022; Altuntaş et al., 2022), following the method described earlier. In brief, a cellulosic dialysis membrane tubing (Spectra-Por4 dialysis tubing, cut off 12–14 kDa, Spectrum Laboratories Inc., New Brunswick, NJ, USA) was loaded with 1 mL of pure RIF aqueous dispersion (RIF = 2 mg) or an equal amount of RIF in LipoRIF dispersion, and then placed in a transparent bottle containing 40 mL of PBS (pH 7.4) as the acceptor medium. The samples were then incubated at 37 °C ± 0.5 °C while being shaken at 40 rpm. The release profiles were analysed using a validated HPLC method as detailed in Section 2.2. The samples were collected at predetermined time intervals (1 h, 2 h, 4 h, 6 h, 24 h, 48 h, 72 h, 96 h, 120 h) and the volume of each sample was immediately replaced with an equal volume of fresh medium. Finally, the cumulative amount of RIF released over time was plotted.

2.4. Preparation and characterisation of freeze-dried LipoRIF

2.4.1. Preparation and optimisation of freeze-dried LipoRIF

LipoRIF dispersion was subjected to a freeze-drying process to convert into a solid formulation (Fig. 1). Briefly, LipoRIF dispersion was first concentrated to eliminate the free drug, as reported in section 2.2.3; LipoRIF concentrated dispersion remained in the Amicon's filters and was collected and frozen at −80 °C for 3 h before the freeze-drying process. Then, the frozen LipoRIF dispersion was freeze-dried for 24 h using a Virtis™ Advantage XL-70 freeze-dryer (SP Scientific, Warminster PA, USA). The lyophilisation process consisted of a primary drying cycle at −40 °C, followed by secondary drying at 25 °C with a vacuum pressure of 50 m Torr. A cryoprotectant was added during the freeze-drying process. Sucrose and trehalose were tested to select the ideal cryoprotectant. The dimensional profile of freeze-dried LipoRIF from each group before and after lyophilisation was recorded as described in section 2.2.2 and used to calculate Sf/Si ratio that indicates nanoaggregate reconstitution. Si and Sf symbolise particle size values before and after lyophilisation, respectively. To do this, freeze-dried LipoRIF was resuspended in 5 mL of deionised water and then vortexed at 2,500 rpm for 30 sec at r.t. Furthermore, particle size and TEM images of the resuspended LipoRIF were evaluated.

2.4.2. Differential scanning calorimetry (DSC)

The thermal properties of pure RIF, Lipoid® S 100, freeze-dried ULipo, LipoRIF and trehalose were determined using Differential Scanning Calorimetry analysis. About 2–5 mg of each sample was weighed in an aluminum pan and sealed before analysis using DSC Q20 (TA Instruments, Elstree, Hertfordshire, UK). The samples were heated at a rate of 10 °C per minute from 10 to 400 °C in a nitrogen atmosphere.

2.4.3. Powder X-ray diffraction (XRD) analysis

Pure RIF, freeze-dried ULipo and LipoRIF and trehalose were subjected to powder XRD analysis to examine their crystallinity. An X-ray
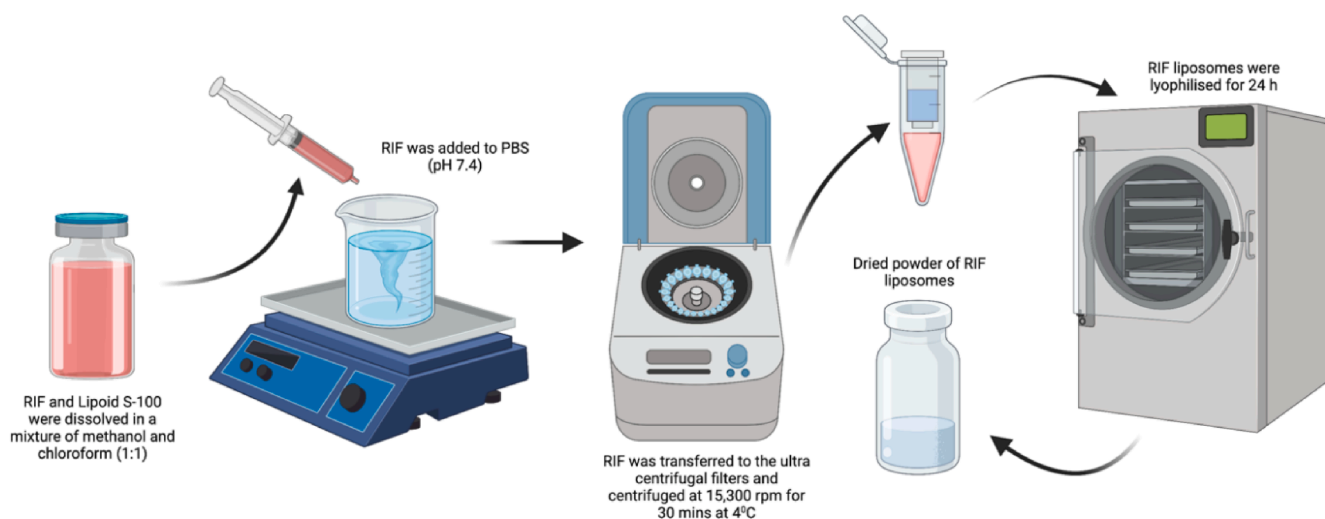
Fig. 1. Schematic illustration of LipoRIF solid preparation.

diffractometer (Rigaku Corporation, Kent, England) was used for the analysis. The scan parameters included a scan range of 0 to 60° (2θ) with a scan speed of 2°/min at 30 kV and 15 mA.

2.4.4. Fourier transform infrared (FTIR) spectroscopy

The chemical interaction between pure RIF, Lipoid S 100, freeze-dried ULipo and LipoRIF and trehalose was determined using an FTIR spectrometer (Accutrac FT/IR-4100TM Series, Perkin Elmer, USA). The spectroscopic scans were observed in the region of 500 to 4000 cm^{-1}.

2.5. Fabrication of DMNs loading freeze-dried LipoRIF

2.5.1. Preformulation study

Two-layered DMNs loading freeze-dried LipoRIF (LipoRIF-DMNs) were fabricated by a casting method (Anjani et al., 2022; Anjani et al., 2022; Anjani et al., 2022), as illustrated in Fig. 2.

The first layer, represented by the DMN tips, was constituted by freeze-dried LipoRIF and an aqueous solution of PVA-PVP (PP2) (1:1 ratio of 40 % w/w each). Three formulations were tested to obtain a first layer with suitable mechanical properties, varying the ratio between freeze-dried LipoRIF and PP2, as outlined in Table 1.

Freeze-dried LipoRIF was mixed with the polymeric solution using a SpeedMixerTM DAC 150.1 FVZ-K (GermanEngineering, Hauschild & Co. KG, Hamm, Germany) at 3,500 rpm for 5 mins. The blend was then poured into a 16x16 silicone mould (pyramidal needles of 850 μm height, 300 μm base width, 300 μm interspacing and 0.36 cm^2 patch

Table 1
Formulations of the first layer of LipoRIF-DMN.

Formulation code	LipoRIF (mg)	PP2 (mg)	Deionised water (mg)
F1	100	100	100
F2	100	200	100
F3	100	300	100

area) and placed in a positive pressure chamber (Protima®, TÜV Rheinlad, Koln, Germany) with a pressure of 5 bar for 5 mins to force the blend to fill the needle cavities. After that, the excess product that remained on the surface of the mould was carefully scraped off, and the mould containing the first layer was further subjected to the positive pressure chamber at 5 bar for 30 mins. Elastomer-based flexible rings were then attached to the top of the mould using an aqueous solution of 40 % w/w PVA (MW 9–10 kDa). The first-layer-filled mould was maintained at ambient conditions overnight to allow the water to evaporate. The day after, the baseplate, consisting of an aqueous blend of 30 % w/w PVP (MW 90 kDa) and 1.5 % w/w glycerol, was cast as the second layer. Furthermore, to enable a better distribution and removal of air gaps, the moulds were centrifuged at 3,500 rpm for 10 mins and were left to dry overnight under ambient conditions. Upon complete drying, the LipoRIF-DMNs were carefully demoulded and the excess baseplate side walls were precisely removed using scissors. The formed LipoRIF-DMNs were dried further at 37 °C for 24 h and later subjected to characterisation.
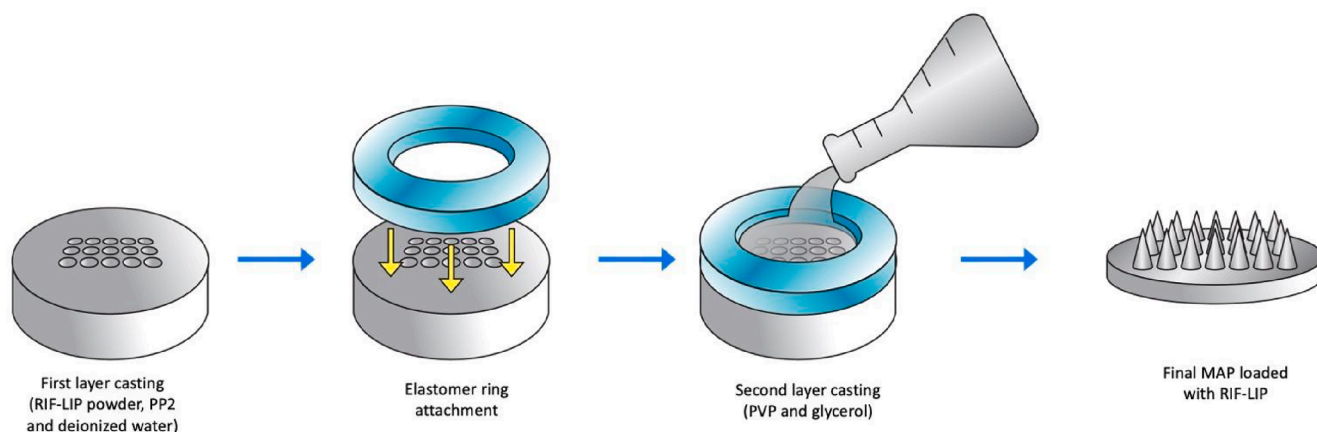

Fig. 2. Schematic illustration of the fabrication of two-layered DMNs loading freeze-dried LipoRIF.

2.5.2. LipoRIF-DMNs visual and mechanical characterisation

The morphology of LipoRIF-DMNs (formulations F1, F2, F3) and the mean needle height estimation were elucidated using a Leica digital light microscope (Leica EZ4 D, Leica Microsystems, Milton Keynes, UK). The compressive resistance of the formulation was determined using a TA-TX2 Texture Analyser (TA) (Stable Microsystems, Haslemere, UK), as previously described (Bin Sabri et al., 2021; Cárcamo-Martínez et al., 2020; Anjani et al., 2022), with a compression force of 32 N for 30 sec at a rate of 0.5 mm/sec to simulate human thumb pressure of patch application ($n = 25$). The compressive resistance of LipoRIF-DMNs was evaluated considering the reduction in needle height post compression and was calculated using Equation (3).

$$Variation\ in\ needle\ height\ (\%) = \frac{\Delta needle\ height}{initial\ needle\ height} \times 100 \qquad (3)$$

Where Δ stands for the difference between needle height before and after the compression test.

The ability of LipoRIF-DMNs to penetrate the skin was assessed both *in vitro* and *ex vivo*. In the *in vitro* experiment, eight layers of Parafilm® M were stacked and the LipoRIF-DMNs (F1, F2, and F3) were inserted into each layer. The extent of insertion was observed under a digital light microscope. In the *ex vivo* experiment, neonatal porcine skin was used to confirm the performance of LipoRIF-DMNs. The insertion of DMN was observed in real-time using an EX-101 optical coherence tomography (OCT) microscope (Michelson Diagnostics Ltd., Kent, UK) and the length of insertion was analysed using ImageJ® software (National Institutes of Health, Bethesda MD, USA). The porcine skin used in the experiment was obtained from stillborn piglets within 24 h after death and was stored at −20 °C until use.

2.5.3. Physical stability of LipoRIF vesicles in LipoRIF-DMNs

LipoRIF-DMNs (F1, F2 and F3) were separately placed in 5 mL of deionized water under stirring at 600 rpm for 1 h at room temperature to dissolve the DMNs. The dimensional profile was evaluated as reported in section 2.2.2 ($n = 3$).

2.5.4. Loading capacity of LipoRIF-DMNs

LipoRIF-DMNs (F1, F2, and F3) were each placed in 4 mL of deionized water and stirred at 600 rpm for 1 h at room temperature to dissolve the hydrophilic polymer. The resulting mixture was then added to 4 mL of methanol and stirred at 600 rpm for 1 h at room temperature to dissolve the drug. After stirring, the mixture was centrifuged at 14,500 rpm for 15 min before analysis using HPLC. Based on the results obtained from these tests, the LipoRIF-DMN formulation with highest drug content was chosen for further evaluations ($n = 5$).

2.5.5. In situ skin dissolution study

In situ skin dissolution was studied to examine the time taken by the LipoRIF-DMNs to dissolve *ex vivo* in the neonatal porcine skin. Here, full-thickness neonatal porcine skin tissue was allowed to attain equilibrium by immersing it in PBS (pH 7.4) for 30 min at 37 °C. LipoRIF-DMNs were manually inserted into the skin using thumb pressure for 30 secs. To avoid dislodging the patch from the skin surface, a cylindrical stainless steel metal weight of approximately 15 g was placed on the top of the MAP. The samples were incubated in an oven (Genlab incubator, Genlab Ltd., Cheshire, UK) with a temperature set at 37 °C and were carefully removed from skin at 5, 15 or 30 min. Finally, LipoRIF-DMNs were examined under the digital microscope.

2.6. Morphological evaluation of LipoRIF-DMNs

The morphology of the chosen LipoRIF-DMNs was examined using a Tabletop Microscope TM3030 (Hitachi, Krefeld, Germany) Scanning Electron Microscope (SEM). SEM images of samples were taken under vacuum conditions at an accelerating voltage of 15 kV. To provide a 3D representation, fluorescence images were obtained using a Leica TCS SP8 multiphoton scanning microscope (Leica Microsystems Ltd, Milton Keynes, UK) equipped with an upright DM6 microscope body and a motorized stage. The Leica Application Suite X software (3.5.7.23225) was used for image acquisitions. Depending on the sample, a water immersion objective HC PL APO CS2 63x with 1.2 Numerical Aperture or dry objectives HC PL FLUOTAR 20X/0.50NA was used for image acquisition. Sample droplets were excited with 850 nm or 900 nm laser lines from the Mai Tai Deep See Mode-Locked laser system (Newport-Spectra Physics, UK), and the fluorescence emission was collected via HyD GaAsP-spectral internal detectors for red dye between 610 nm and 764 nm. Fluorescence images were collected at a 512x512 or 1024x1024 pixel resolution format and 400 Hz or 600 Hz scanner speed. Optical sections of the specimen between 300 μm and 1000 μm deep into the tissue were taken with the distance between the images in the z-stack between 5 μm or 10 μm. Brightfield images were collected in parallel with the fluorescence images using the PMT (Photomultiplier tube) detector and excitation of the MaiTai laser at 850 nm or 900 nm. Tile scan images were taken for 2000 μm × 3400 μm across the specimen to determine the distribution of the drug in the tissue. Image analysis was performed using the Leica Application suite X software (3.7.020979). Additionally, the TEM images of redispersed LipoRIF from LipoRIF-DMNs were taken, and films were prepared by mixing LipoRIF and polymer using the same ratio for the first layer of DMNs formulation to understand the nature of "bulges" forming on the surface of needles. The morphology of the films was evaluated using an optical microscope and SEM.

2.7. Storage stability of LipoRIF-DMNs

The storage of the leader LipoRIF-DMNs was evaluated regarding needle height reduction and RIF content over time after storing samples at 25 °C/RH 65 % in the stability chamber (Binder GmBH, Tuttlingen, Germany) (Anjani et al., 2023; Anjani et al., 2023). It was analysed at each predetermined time point (7, 14, 30, 60 and 90 days). Needle height reduction and RIF content were evaluated as reported in sections 2.5 and 2.6, respectively. For assessing the stability of LipoRIF-DMNs at accelerated conditions, the samples were stored at 40 °C/RH 75 % in the stability chamber and were analysed at 30 days ($n = 4$).

2.8. Ex vivo dermatokinetic study

The delivery efficiency of RIF to different layers of full-thickness neonatal porcine skin was assessed using a Franz cell diffusion apparatus (PermeGear, Inc., Hellertown, PA, USA). LipoRIF-DMNs, containing approximately 75 μg of RIF, and a LipoRIF dispersion (1.5 mL, containing approximately 100 μg of RIF) were evaluated separately. First, the full-thickness neonatal porcine skin was trimmed to fit the donor compartment of the Franz cells and glued with cyanoacrylate glue (Stick it® super glue, PLDZ Pattison House, Dublin, ROI) with the subcutaneous side facing the receiver compartment. LipoRIF-DMNs were manually inserted into the skin (*stratum corneum* side) using thumb pressure for 30 sec. The receiver compartment of the Franz cells was filled with PBS (pH 7.4) as the receiver medium and covered with a thermal water jacket to maintain the receiver temperature at 37 °C to simulate physiological conditions, and the medium was continuously stirred using metal bars at 600 rpm. Finally, a metal clamp was used to attach the donor and receiver compartments, followed by the placement of a cylindrical stainless steel metal weight on top of the LipoRIF-DMNs to prevent their expulsion from the skin during the experiment. Both skin and receiver compartments were collected at 1, 3, 6, 12, and 24 h. The samples from the receiver compartment were centrifuged at 15,300 rpm for 15 min, filtered using a 0.45 μm PTFE membrane filter and analysed for RIF content using HPLC. The skin samples were also collected at these time intervals. They were heated at 60 °C on a hot plate to separate the epidermis and dermis layers of the skin, and then the separated layers were processed individually. The epidermis layer

was homogenized with 2 mL of methanol as removing solvent for 30 min using a thermal mixer (ThermoMixer F2.0, Eppendorf, Hamburg, Germany) to extract RIF. On the other hand, the dermal layer was first homogenized in 0.5 mL deionised water using Tissue Lyser LT (Qiagen Ltd., Manchester, UK) at 50 Hz for 15 min. Then, 1 mL of methanol was added to the above mix and homogenized following the same protocol. All the epidermis and dermis samples were centrifuged at 15,300 rpm for 15 min, and the collected supernatant was used for HPLC analysis.

2.9. Biocompatibility study

The compatibility of LipoRIF-DMNs and ULipo with fibroblast cells from mice (ATCC CRL-3242) was assessed for biocompatibility. Fibroblasts were seeded at a concentration of 3000 cells per square centimetre in DMEM (Dulbecco's Modified Eagle's Medium) (Sigma-Aldrich, St. Louis, USA), with 2 % (w/v) L-glutamine, 10 % (v/v) fetal bovine serum (FBS) (Gibco, Thermo Fisher Scientific, Waltham, Massachusetts, USA) and 1 % (v/v) antibiotic–antimycotic, until confluence at 37 °C with a 5 % CO_2 atmosphere. Sterilised LipoRIF-DMNs and ULipo were treated with a solution of 0.25 % (w/v) trypsin and 0.53 mM ethylenediaminetetraacetic acid (EDTA) before introduction to the cell lines. The samples were then incubated with the formulations and evaluated using a cell viability test, live and dead assay and a cell proliferation test. The MTT (3-[4,5-dimethylthiazol-2-yl]-2,5 diphenyltetrazolium bromide) assay was used for the cell viability test, as previously described in a study (Anjani et al., 2022; Anjani et al., 2022; Anjani et al., 2023). After three days of culture over the ULipo-DMNs or LipoRIF-DMNs, the cell-seeded samples were washed with PBS (pH 7.4) to remove the remaining DMEM. Then, 0.5 g/L of MTT stock solution was added to each well in a 96-well plate and incubated for 5 h at 37 °C with a 5 % CO_2 atmosphere until crystals formed. Subsequently, the MTT solution was removed, and crystals were diluted with dimethyl sulfoxide (DMSO) (Sigma-Aldrich, Saint Louis, USA). The absorbance was read at 570 nm on a Synergy H1 microplate reader (Agilent Technologies, St. Clara, USA). Fibroblast cells seeded with no tested materials were used as a control positive, and Triton X-100 (1 %) was used as a negative control. The ULipo-DMNs or LipoRIF-DMNs toxicity over the fibroblast cells was confirmed by a live/dead assay. The protocol for live/dead staining was previously described. Briefly, the ULipo-DMNs or LipoRIF-DMNs were washed with PBS (pH 7.4) and then stained for 5 min at room temperature in 5 μg/mL calcein AM (a marker for living cells) and 5 μg/mL ethidium homodimer-1 (a marker for dead cells) (Molecular probes, Eugene, Oregon). Fluorescence images were taken using an Olympus Fluoview Confocal Microscope. The PicoGreen® assay (Invitrogen, Thermo Scientific, Waltham, MA, USA) was used to evaluate cell proliferation for all MAPs conditions (ULipo-DMNs and LipoRIF-DMNs) following the manufacturer's guidelines. A standard curve of known DNA concentrations was made to determine DNA content. After a 5-min room temperature incubation, sample fluorescence was read on a Synergy H1 microplate reader (Agilent technologies, St, Clara, USA) with an excitation at 480 nm and emission at 520 nm (n = 3).

2.10. In vitro antibacterial activity of LipoRIF-DMNs

Lipo-RIF DMNs were examined for their ability to prevent the growth of MRSA NCTC 33592 (National Collection of Type Cultures, Salisbury, UK). To prepare for the microbiological assessments, MRSA strains were stored in Mueller Hinton (MH) broth with 15 % glycerol at −80 °C and grown in MH broth at 37 °C for 48 h when needed. The *in vitro* microbial assay followed methods published previously (Peng et al., 2021; Anjani et al., 2022; Bin Sabri et al., 2023) but with some modifications. The MRSA culture was first incubated at 37 °C and 100 rpm overnight in Mueller Hinton (MH) broth. Then, 50 μL of this culture was added to 5 mL of soft MH agar and immediately vortexed before pouring onto an MH agar plate, providing sufficient bacterial coverage for inter-group comparisons in the experiment. RIF-LIP loaded DMNs were placed in

the center of the MH agar plate and incubated at 37 °C for 24 h. Additionally, plates with MRSA alone as a positive control, unloaded DMNs, and ULipo-DMNs as a negative control were also set for 24 h at 37 °C. The zone of inhibition diameter for MRSA was measured in mm (n = 5).

2.11. Statistical analysis

The results were analysed and interpreted using GraphPad Prism® version 9.4 (GraphPad Software, San Diego, California, USA). When comparing multiple groups, one-way analysis of variance (ANOVA) was performed, and statistical significance was defined as $p < 0.05$. In addition, statistical significance was indicated using the symbols * for > 0.05, ** for > 0.01, and *** for > 0.001. Unless stated otherwise, the data are presented as means ± standard deviation (SD).

3. Results and discussion

3.1. Formulation and characterisation of LipoRIF dispersion

Formulation of liposomes often involves the influence of numerous factors, from formulation design to process parameters (Ghodake et al., 2020; Dhoble and Patravale, 2019). To consider all the possible factors that would determine ideal liposome formation, LipoRIF dispersion was optimised using a Box Behnken design in DoE software, which suggested 15 formulations. Particle size, PDI and drug entrapment were recorded as the responses for all formulations, presented in **Table S2** (Supplementary data). The representative 3D surface graphs detailing the effect of parameters on the particle size, PDI and entrapment efficiency are displayed in Fig. 3. The optimum formulation was chosen based on the highest desirability factor for particle size in the range of 200–400 nm, minimum PDI and maximum drug entrapment, as generated by the software. The optimised formulation was determined to have the drug to lipid ratio of 1:10, the quantity of solvent used was 2.590 mL, and the magnetic stirring rate was 1,190 rpm. The bias between the predicted and observed values were less than 15 % in all cases. Experimentally, LipoRIF dispersion and the comparable unloaded one (ULipo dispersion) were milky, and no aggregation or phase separation phenomena were detected. The observed characteristics of LipoRIF and ULipo dispersions are reported in Table 2 and morphology is illustrated in Fig. 4.

The size and distribution of loaded and unloaded formulations proved that nanovesicles were monodisperse in the nanosize range (size < 500 nm; PDI < 0.4). Recorded RIF loading in LipoRIF dispersion was about 80 μg/mL, where 83 % was entrapped in LipoRIF vesicles. The mean size of ULipo significantly increased following RIF loading ($p < 0.01$); still, the dimensional homogeneity was not affected ($p > 0.05$). Furthermore, TEM micrographs illustrate a morphological variation between LipoRIF and ULipo vesicles, evidencing a difference in lipid lamellar arrangement.

Liposome-like vesicles are very challenging to study since individual lipid bilayers are undetectable by traditional light microscopy. They are very delicate due to weak non-covalent interactions (Wu et al., 2014). Assuming this, statistical observations regarding ULipo and LipoRIF size and detected variations in terms ofmorphology suggest RIF's role in the formation of liposomes. The solvent injection method was employed to form liposomal-like vesicles (Fig. 5), which provides advantages like protection of phospholipids from oxidation and degradation, imparts better liposome stability and monodispersity and avoids the need for additional size reduction processes that may occur with thin film hydration techniques (Gouda et al., 2021). Moreover, this method was selected due to its simplicity, required short manufacturing time and ease to scale-up (Wagner and Vorauer-Uhl, 2011; Charcosset et al., 2015).

The current procedure involves the injection of an organic phase (solvent) into a relatively large volume of water phase (non-solvent). Since RIF is a lipophilic compound (Log P = 2.7), it was dissolved in the organic phase. When the organic phase is injected into the aqueous
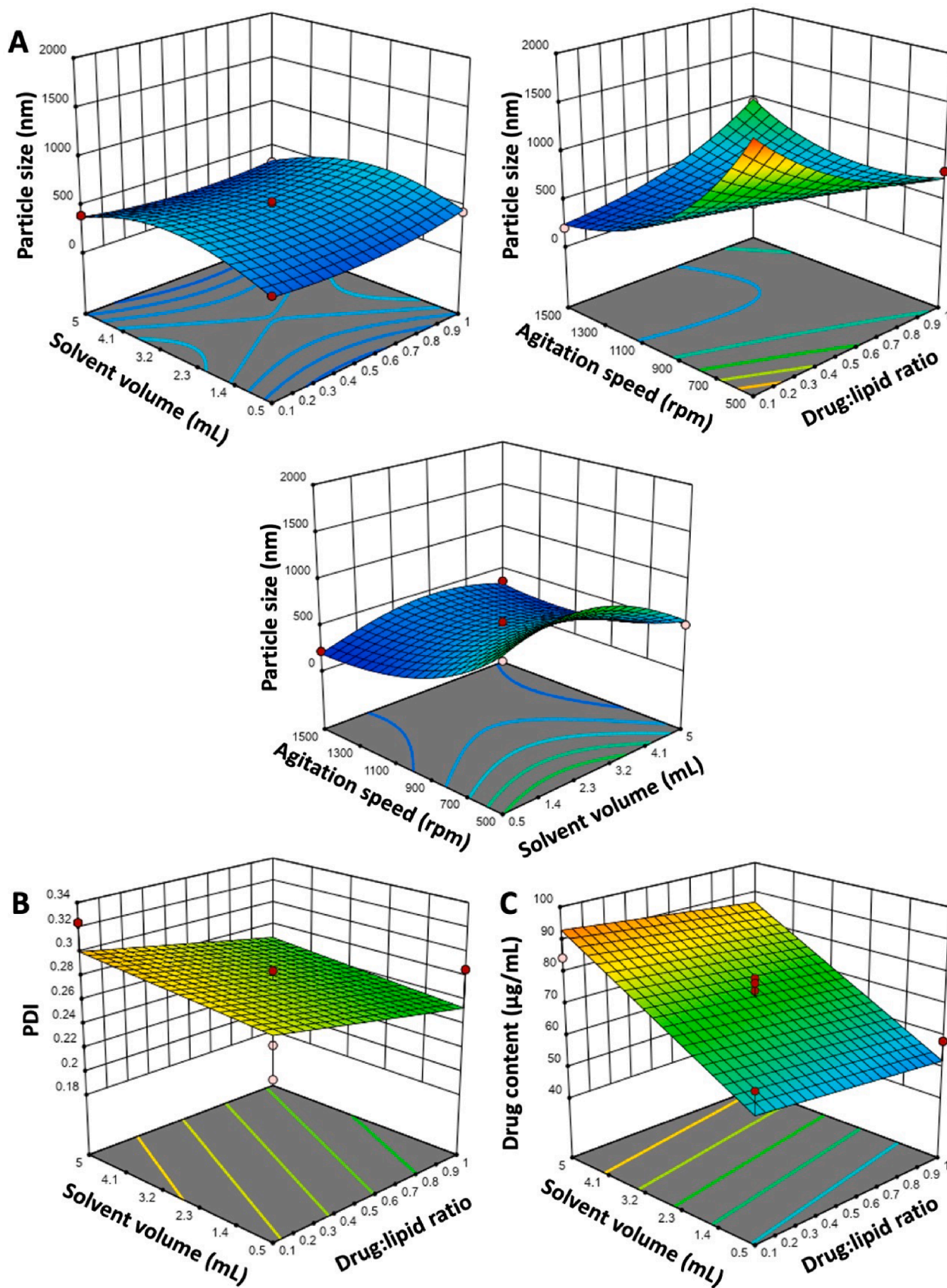
Fig. 3. Response surface plots describing the effect of the drug: lipid ratio, solvent volume and agitation speed to the (A) particle size and (B) PDI and (C) drug entrapment of LipoRIF formulation.

Table 2
Observed characteristics of LipoRIF and ULipo dispersions.

Formulation	Size (nm)	PDI	RIF loading (µg/mL)	EE %
LipoRIF dispersion	226.42 ± 23.98**	0.288 ± 0.010	81.09 ± 2.25	83.76 ± 0.87
ULipo dispersion	183.73 ± 4.9	0.212 ± 0.011	–	–

EE: entrapment efficiency. Results are expressed as means value ± standard deviation (n = 3). ** p value < 0.01 vs Ulipo dispersion.

phase (PBS pH 7.4), the phospholipids are exposed to an unfavourable environment, leading to the arrangement of phospholipid bilayer fragments. These fragments then fuse together after the organic solvent is evaporated, in order to reduce their exposure to water. If the bilayer fragments are enough fluids to favour their spontaneous bending, the fragment fusion will result in unilamellar and spherical vesicles (Wagner and Vorauer-Uhl, 2011; Gouda et al., 2021). On the contrary, if fragments present a more rigid structure, their high-energy required bending will result in multilamellar vesicles (Wagner and Vorauer-Uhl, 2011; Gouda et al., 2021). The fluidity of the bilayer is mainly governed by the lipid packing parameter and the temperature employed during the formulation process (Wu et al., 2014; Israelachvili et al., 1976). Herein, LipoRIF were prepared at ambient temperature to prevent RIF degradation (Sutradhar and Zaman, 2021). When liposomes are prepared below the phospholipoid transition temperature, nonspheroidal aggregates may be developed upon crystallisation of the lipids (e.g., polygon-shaped vesicles, faceted vesicles, disks, etc.) (Wu et al., 2014). However, ULipo vesicles appeared to be unilamellar spheres. In the case of LipoRIF, larger multilamellar (MLV) and polygon-shaped vesicles were observed. Hence, the formation of MLV was hypothesized to be a consequence of the RIF loading, which is likely to intercalate in the
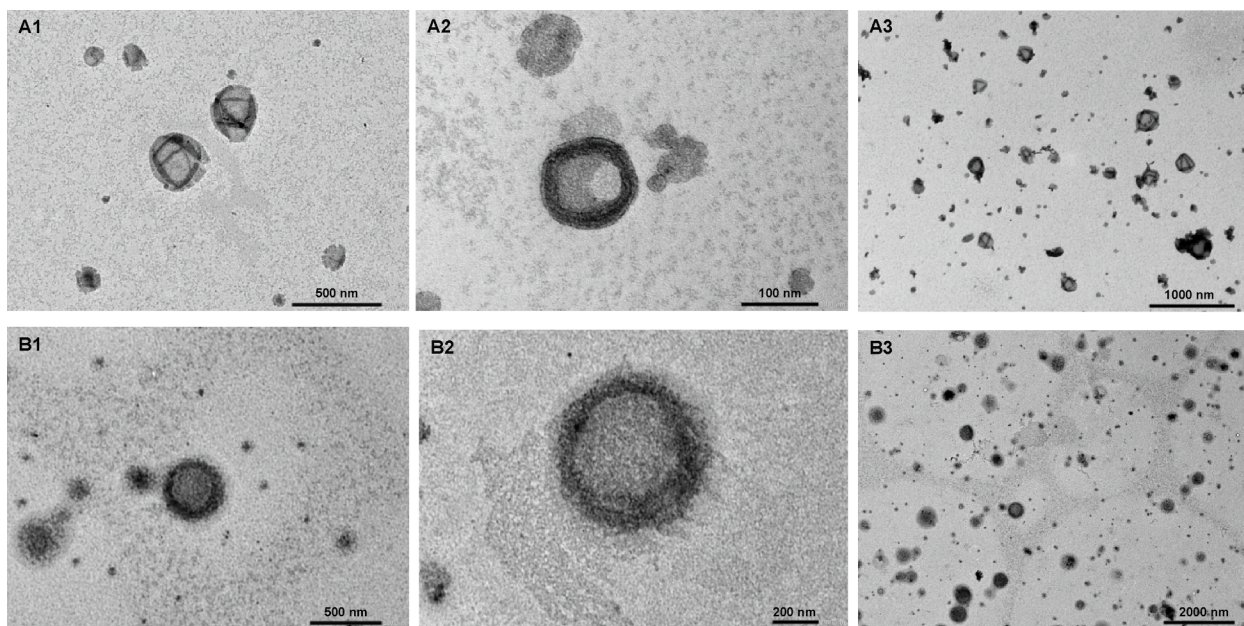

Fig. 4. TEM micrographs of LipoRIF dispersion (A) and ULipo dispersion (B).
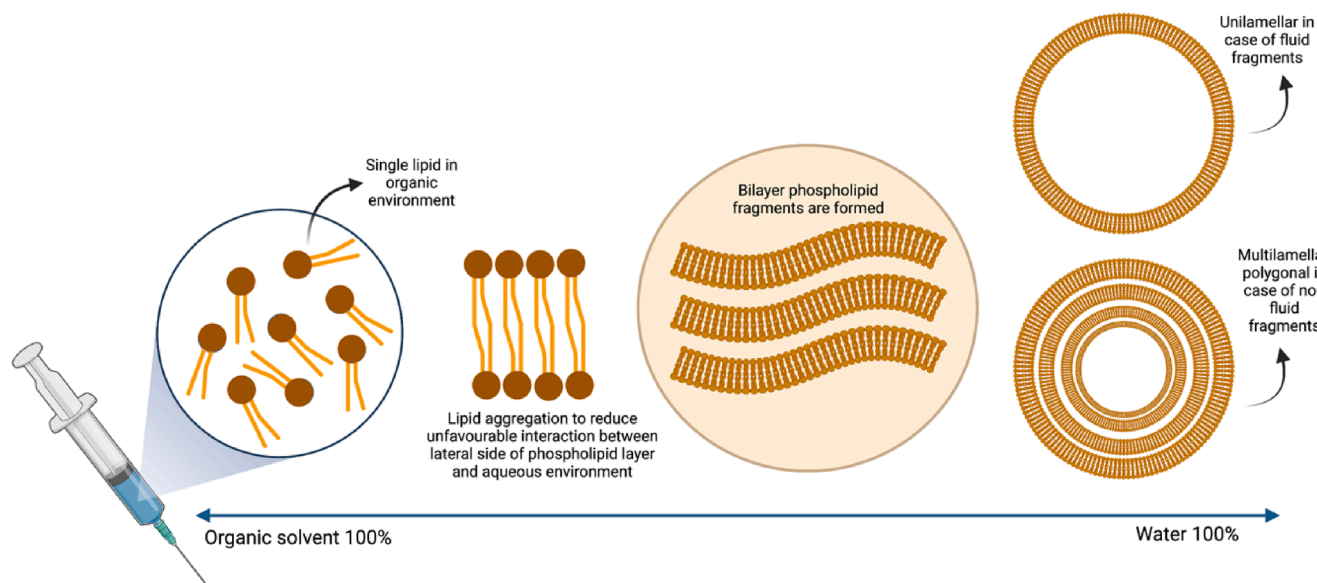

Fig. 5. Phospholipid bilayer forming upon injection of organic phase to an aqueous phase.

hydrophobic palisade of the phospholipid bilayer, thus modifying the effective lipid packing parameter $P = v/a_0l_c$, where v represents the volume of the hydrophobic chain, a_0 is the headgroup area, and lc is the critical hydrocarbon chain length. Such alteration of P can undoubtedly play a role in the different behaviours of liposomes regarding fluidity, determining the characteristics of the vesicles (Demartis et al., 2021; Israelachvili et al., 1976). Further proof of the different fluidity of ULipo and LipoRIF vesicles was confirmed in the flexibility degree investigation (**Figure S1**, supplementary data).

The *in vitro* release profile of RIF from LipoRIF dispersion was evaluated and compared to an aqueous dispersion of pure RIF, maintaining the same RIF amount. The cumulative amount of RIF released in the acceptor medium is reported in Fig. 6. LipoRIF dispersion provided a 44.67 ± 1.42 % RIF release within 24 h. No further RIF was detected in the acceptor medium for the rest of the experiment ($p < 0.0001$ vs RIF at 24 h; $p > 0.05$ vs RIF at 120 h). On the other side, pure RIF dispersion could actively release 84.84 ± 2.27 % of RIF over 72 h, and no significant amount of RIF was released in the following time ($p < 0.001$ vs RIF at 24 h; $p > 0.05$ vs RIF at 120 h). Focusing on the first 24 h, a RIF burst release was evident in the case of pure RIF. Notably, 56.24 ± 4.23 % of RIF was released after 6 h to reach 67.31 ± 3.76 % at 24 h ($p > 0.05$). Conversely, the release from LipoRIF dispersion was more controlled, as 26.65 ± 2.25 % of RIF was released within 6 h to reach the *plateau* phase at the next time point.

RIF is a lipophilic compound soluble in organic solvents; its solubility in an aqueous medium is pH dependent. In a previous publication by the same authorship, RIF exhibited a solubility of 0.31, 0.87, and 1.40 mg/mL at pH 4.0, 7.0 and 9.0, respectively (Anjani et al., 2021). This property mainly explains the outcomes of the *in vitro* release study. Due to the slightly basic pH of the buffered medium used, the dispersion released about 85 % lipophilic RIF, which quickly migrated to the aqueous phase. In contrast, when the LipoRIF dispersion is employed, only 40 % of RIF migrated to the aqueous phase, and the rest remained associated with the liposomal lipid bilayer up to the time tested. According to the literature, the strong interaction of RIF–lipid improves the biopharmaceutical profile of RIF (Singh et al., 2014); furthermore, it is highly beneficial for microbial eradication, as liposomal vesicles were reported to interact with the microbial cell membrane, improving cellular drug uptake (Gonzalez Gomez and Hosseinidoust, 2020).

Storage stability of LipoRIF dispersion was evaluated by recording the size and distribution of the vesicles at 25 °C/65 % RH over three months (Fig. 7). The particle size remained stable, while PDI varied through the study, evidencing aggregation-disaggregation-like phenomena. Accelerated stability of LipoRIF dispersion was tested at 40 °C for 30 days (González-González et al., 2022); however, no significant variations in particle size or PDI were reported ($p > 0.05$). In addition, the chemical stability of RIF in LipoRIF dispersion was analysed as drug loading over three months, and no significant variations were observed ($p > 0.05$). This result confirms that the LipoRIF dispersion is physically and chemically stable.

3.2. Formulation and characterisation of freeze-dried LipoRIF

Aiming to include LipoRIF vesicles into DMNs, the current liquid formulation was not the best to favour an easy inclusion process. In this regard, a previous study including transfersomes in DMNs by the same authorship revealed that a liquid dispersion could affect the performance of the final formulation in terms of drug content (Demartis et al., 2022). Therefore, we decided to include LipoRIF in DMNs in a solid form obtained with a freeze-drying process. A cryoprotectant must be added to maintain similar particle size and distribution after the freeze-drying-rehydration cycle (El-Nesr et al., 2010). Sucrose and trehalose at different concentrations were investigated for their ability to protect liposomes against fusion and leakage during lyophilization processes (El-Nesr et al., 2010). To determine the aggregation post reconstitution in water, Sf/Si ratio was calculated by comparing the final particle size after freeze drying (Sf) and particle size before freeze drying (Si) (Ghodake et al., 2020). The results reported in Table 3 indicate that sucrose and trehalose 1 % w/v did not prevent the aggregation of liposomes resulting in microparticles after the freeze-drying-rehydration cycle. Trehalose, 3 % w/v, has an optimal Sf/Si value (Sf/Si < 1.5) and was selected as cryoprotectant for freeze-dried LipoRIF (Ghodake et al., 2020). Micrographs of redispersed freeze-dried LipoRIF are illustrated in Fig. 8.

DSC and XRD analysis were carried out to study the crystallinity state of RIF in freeze-dried—LipoRIF, which are presented in Fig. 9**A** and Fig. 9**B**, respectively. DSC thermograms of pure RIF showed a sharp exothermic signal at 259 °C, representing the decomposition of RIF, as previously reported (Anjani et al., 2021; Agrawal and Panchagnula, 2004; Alves et al., 2010). However, this exothermic peak was not observed in the LipoRIF formulation, which suggests the drug was successfully interacting with the liposome. Moreover, XRD analysis was conducted to verify the DSC result. The diffractogram of pure RIF displayed several sharp peaks, which indicates that RIF is present in a crystalline form. The disappearance of these peaks in the LipoRIF samples confirmed that RIF had successfully entered the liposome. Fig. 9**C** shows the FTIR spectra of pure RIF, pure Lipoid S 100®, pure trehalose, freeze-dried ULipo and LipoRIF. Interestingly, the spectrum of ULipo was similar to LipoRIF, and all the characteristic peaks in pure Lipoid S-100® spectra were also found in both ULipo and LipoRIF. This result is in concordance with the DSC thermogram and XRD analysis, which confirm that RIF has been encapsulated in the liposomal vesicle.
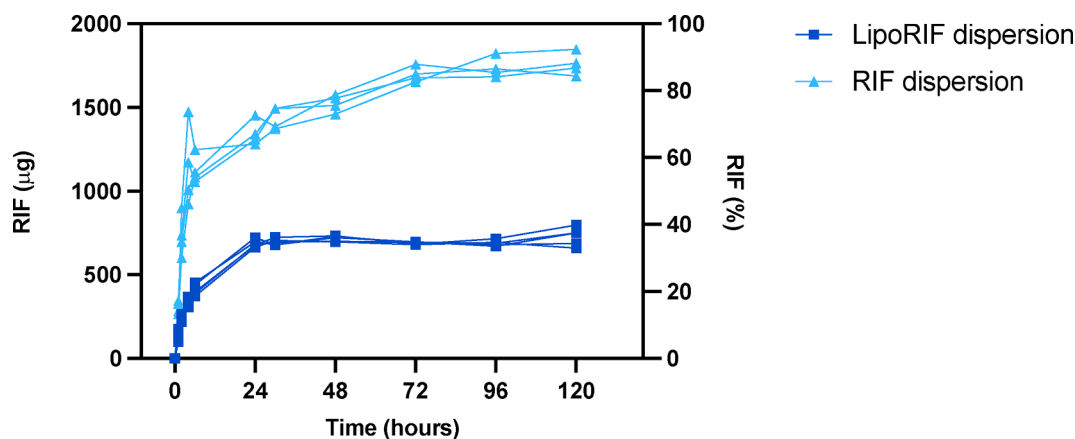

Fig. 6. *In vitro* release profiles of RIF from LipoRIF dispersion and pure RIF dispersion ($n = 4$).
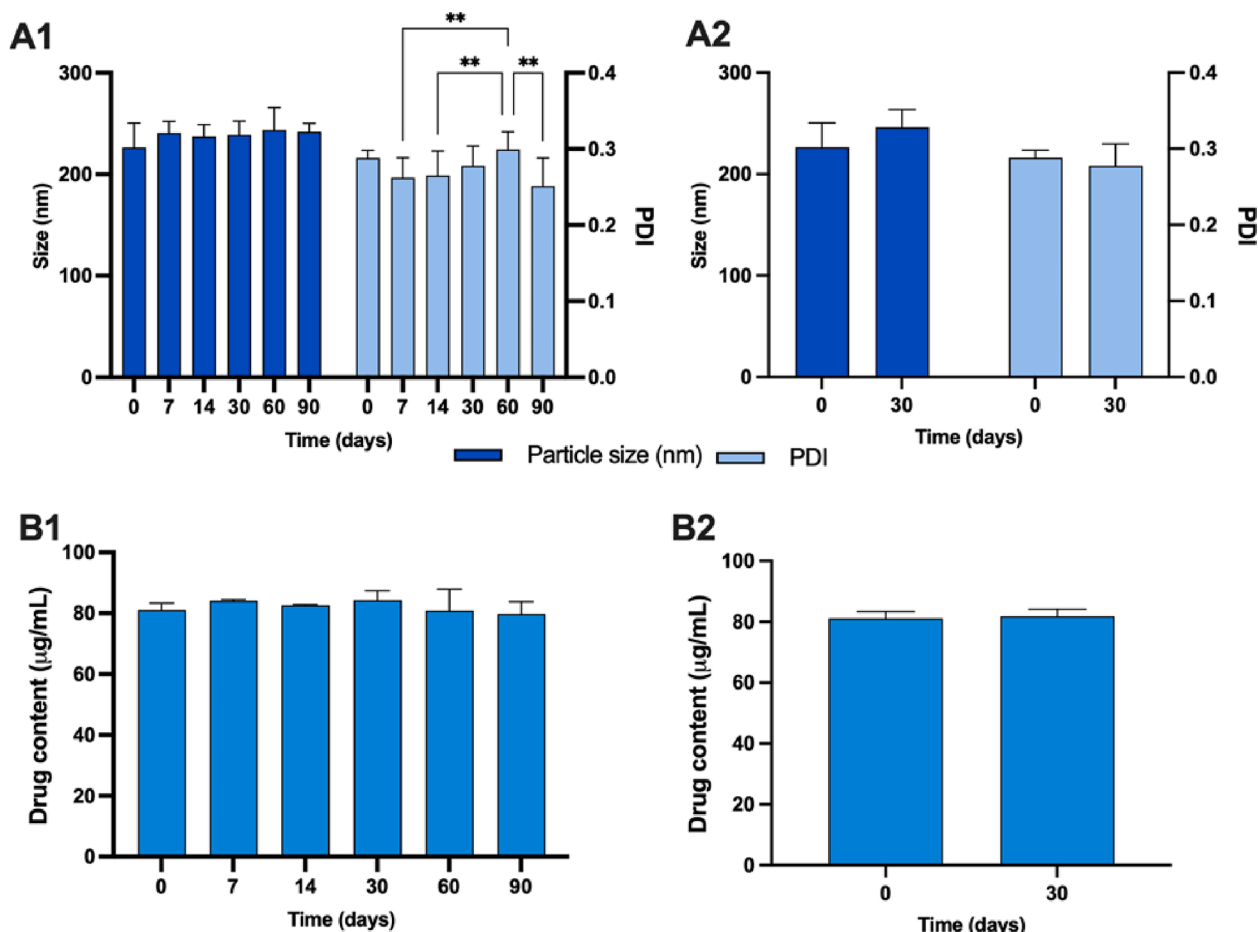
Fig. 7. (A) Storage stability of LipoRIF dispersion at (1) 25 °C/65 %RH and (2) 40 °C/75 %RH expressed in terms of size and dimensional distribution variation and (B) drug content. (means + SD, $n = 9$) ** p value < 0.01.

Table 3
Dimensional profile of freeze-dried LipoRIF in the function of the type and amount of cryoprotectant used (means ± SD, $n = 9$).

Cryoprotectant	% w/v	Size (nm)	PDI	Sf/Si
Sucrose	1	2564.92 ± 317.92	0.453 ± 0.063	6.88
Trehalose	1	870.68 ± 76.27	0.331 ± 0.046	2.33
Trehalose	2	489.03 ± 24.68	0.289 ± 0.040	1.31
Trehalose	3	381.58 ± 18.46	0.298 ± 0.022	1.02

3.3. Fabrication and characterisation of LipoRIF-DMNs

3.3.1. Preformulation study

Three formulations of two-layered LipoRIF-DMNs were prepared by the casting method (F1, F2, F3), varying the ratio between the amount of the freeze-dried LipoRIF and the polymer blend. The three formulations did not differ in morphology (Fig. 10); they resulted in 256 pyramidal-shaped MNs with a height of 850 μm, bubble-free, sharp, and uniformly distributed on the patch area. LipoRIF (orange-coloured) is visually located in the first layer, represented by the tips. This indicates the successful use of the fabrication method to manufacture consistently defect-free DMNs.

LipoRIF were integrated into DMNs to deliver LipoRIF to the target site (epidermis and dermis) to interact with microbial cells and favour the eradication of SSTIs. Thus, it is essential to define RIF loading and to assure the physical stability of LipoRIF vesicles in LipoRIF-DMNs. RIF loading in LipoRIF-DMNs and the dimensional profile of LipoRIF vesicles released from each formulation are reported in Table 4.

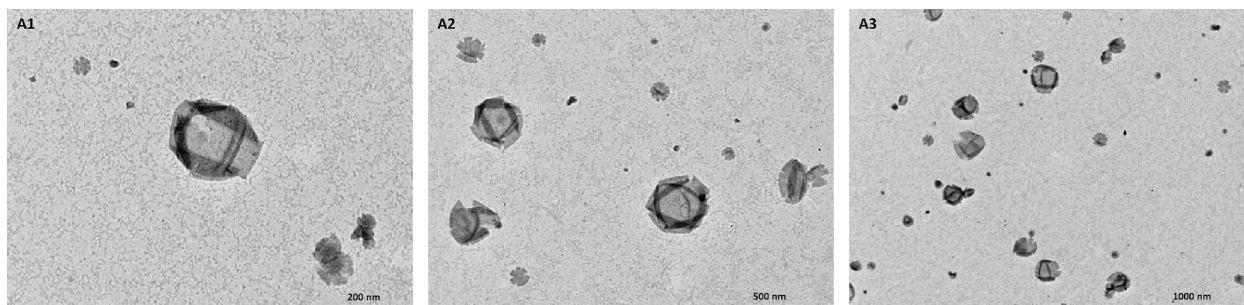Concerning dimensional profile, particles around 300–350 nm,

Fig. 8. TEM micrographs of selected freeze-dried LipoRIF (trehalose 3% w/v).
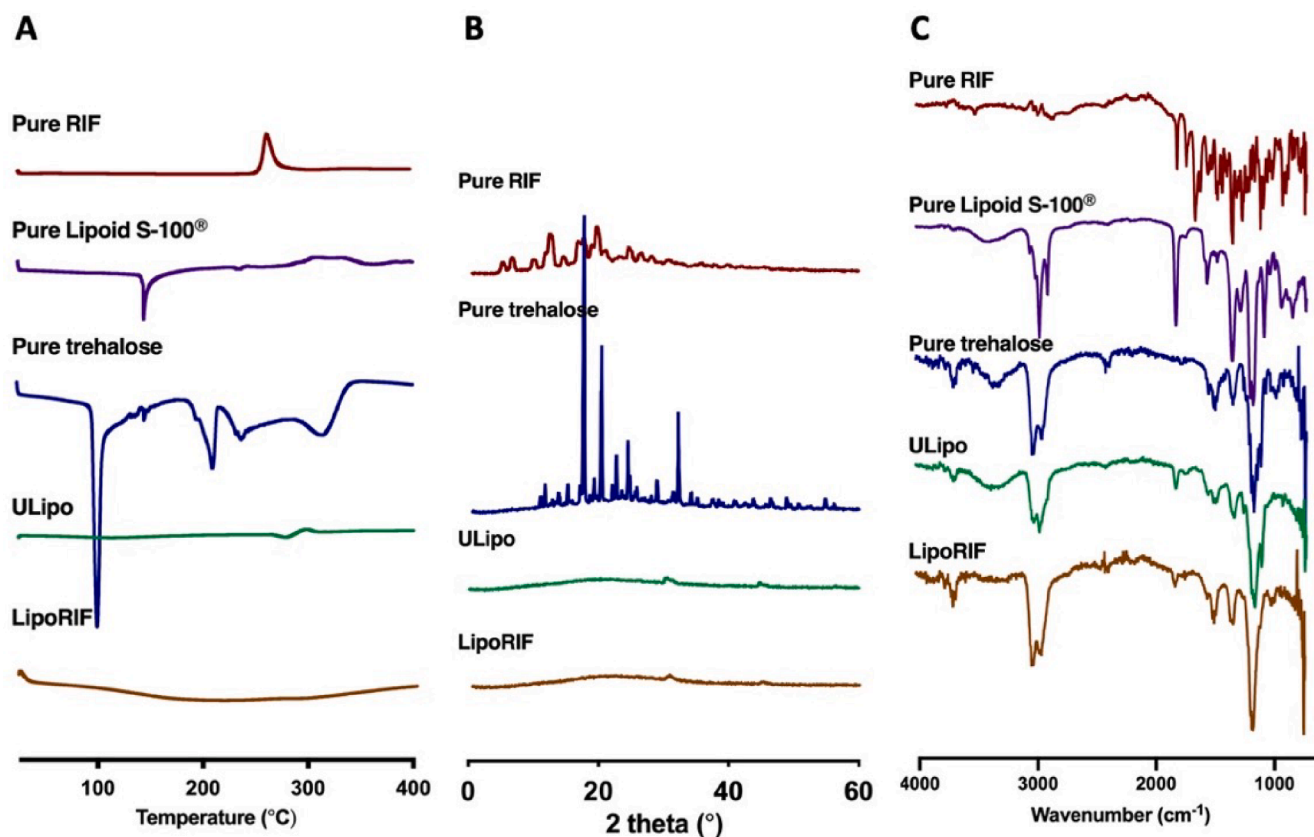
Fig. 9. (A) Differential scanning calorimetry thermogram of pure RIF, pure Lipoid S-100®, pure trehalose, freeze-dried ULipo and LipoRIF. (B) Powder X-ray diffraction of pure RIF, pure trehalose, freeze-dried ULipo and LipoRIF. (C) Fourier transform infrared analysis of pure RIF, pure Lipoid S-100®, pure trehalose, freeze-dried ULipo and LipoRIF.
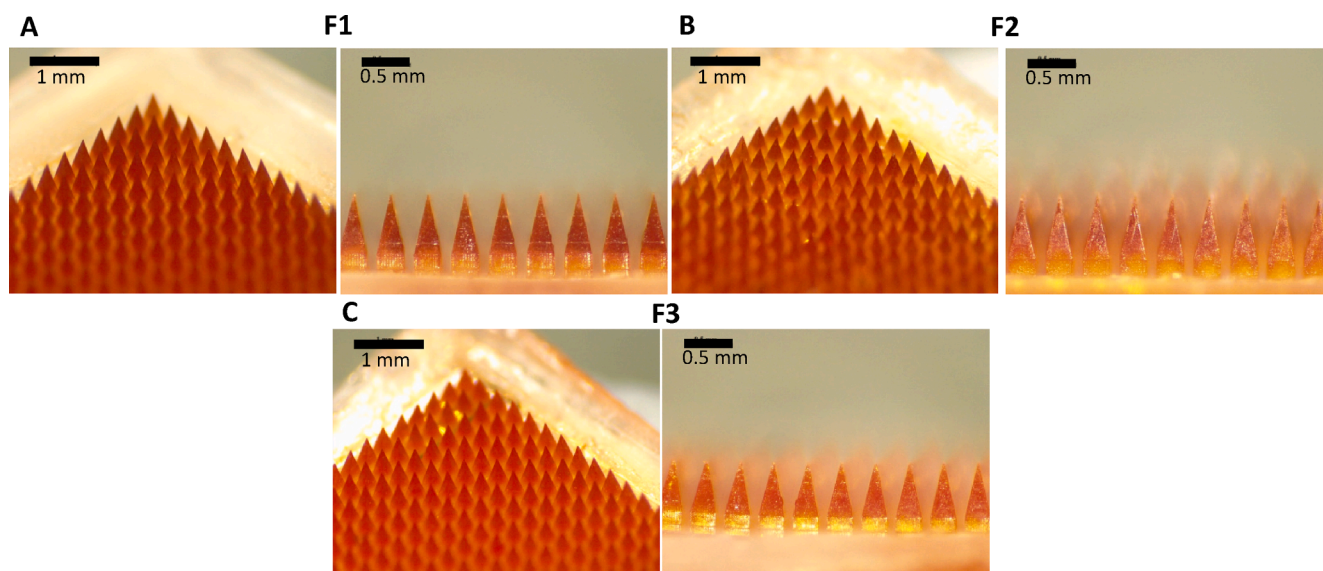

Fig. 10. Pictures of LipoRIF-DMNs acquired at optical microscopy: (A) F1, (B) F2 and (C) F3.

homogenously distributed, were obtained for all three formulations tested. Recently, Shinde *et al.* (Shinde et al., 2019) demonstrated that nanostructured lipid carriers of 300 nm size enabled more significant amounts of drug to enter and be retained in the skin, simultaneously minimising systemic exposure (Shinde et al., 2019). Similarly, Liu *et al.* (Liu et al., 2021). discussed an investigation concerning size-dependent liposome absorption through the skin, evidencing how the transdermal

absorption for sub-100 nm particles was higher than that of larger liposomes with 200 nm to 300 nm diameters. The small size favours the travel through the intercellular gaps inside the brick-and-mortar *stratum corneum* structure; conversely, larger liposomes are less likely to penetrate through those gaps, independently of the size difference within this range (Liu et al., 2021). Based on these assumptions, the resulting particle size of redispersed LipoRIF was considered appropriate for the aim

Table 4
RIF loading and redispersed LipoRIF dimensional profile of F1, F2 and F3 LipoRIF-DMNs in the function of LipoRIF to polymer ratio, compared to freeze-dried LipoRIF.

Formulation	LipoRIF: polymer	RIF loading (µg)	Dimensional profile of Redispersed LipoRIF	
			Size (nm)	*PDI*
Freeze-dried LipoRIF	–	–	381.58 ± 18.46	0.298 ± 0.022
F1 LipoRIF-DMNs	1:1	74.05 ± 4.47	334.29 ± 18.23*	0.281 ± 0.019
F2 LipoRIF-DMNs	1:2	57.85 ± 4.04	330.64 ± 20.48**	0.263 ± 0.036
F3 LipoRIF-DMNs	1:3	47.90 ± 2.32	326.08 ± 35.93**	0.217 ± 0.021

Values are expressed as the average ± standard deviation of three independent measurements for each formulation (n = 3). * $p < 0.01$ and ** $p < 0.001$ compared to freeze-dried LipoRIF.

of the study.

Regarding quantitative determination, the RIF loading was in the range of 45.58—78.52 µg per patch and was observed to decrease while the ratio between LipoRIF and the polymer blend increased. This

phenomenon can be attributed to the higher viscosity of blends incorporating a more substantial amount of LipoRIF, which may result in greater resistance in filling the micro-mould (Demartis et al., 2022).

Results of *In vitro* and *ex vivo* mechanical testing of F1, F2 and F3 is displayed in Fig. 11. The MNs height of the three formulations significantly decreased following the compression test ($p < 0.0001$) (Fig. 11**A**). The recorded percentage height reduction was 9.42 ± 3.17 % for F1, 13.40 ± 3.19 % for F2 and 12.96 ± 6.17 % for F3, with the lowest reduction observed for F1. (F1 vs. F2 $p < 0.01$; F1 vs. F3 $p < 0.01$; F2 vs. F3 $p > 0.05$). It is worth noting that, by increasing the ratio of LipoRIF to polymer, an increase in the percentage height reduction of the DMNs was observed. It is postulated that this may be due to the proportion of LipoRIF in the formulation, which affects the mechanical strength of the needles. This has been previously reported that the phospholipid bi-layers can be converted into a two-dimensional rigid crystalline state at a cooler temperature (Alberts et al., 2008). In this case, the tails of saturated fatty acid will unite and pack tightly together, forming a dense vesicle, resulting in better mechanical strength for the DMNs formulation. Nevertheless, the fabricated LipoRIF-DMNs had sufficient mechanical strength to resist compression, with the percentage of needle height reduction less than 15 % (Anjani et al., 2022; Anjani et al., 2022).

To evaluate the skin insertion ability of LipoRIF-DMNs, eight layers
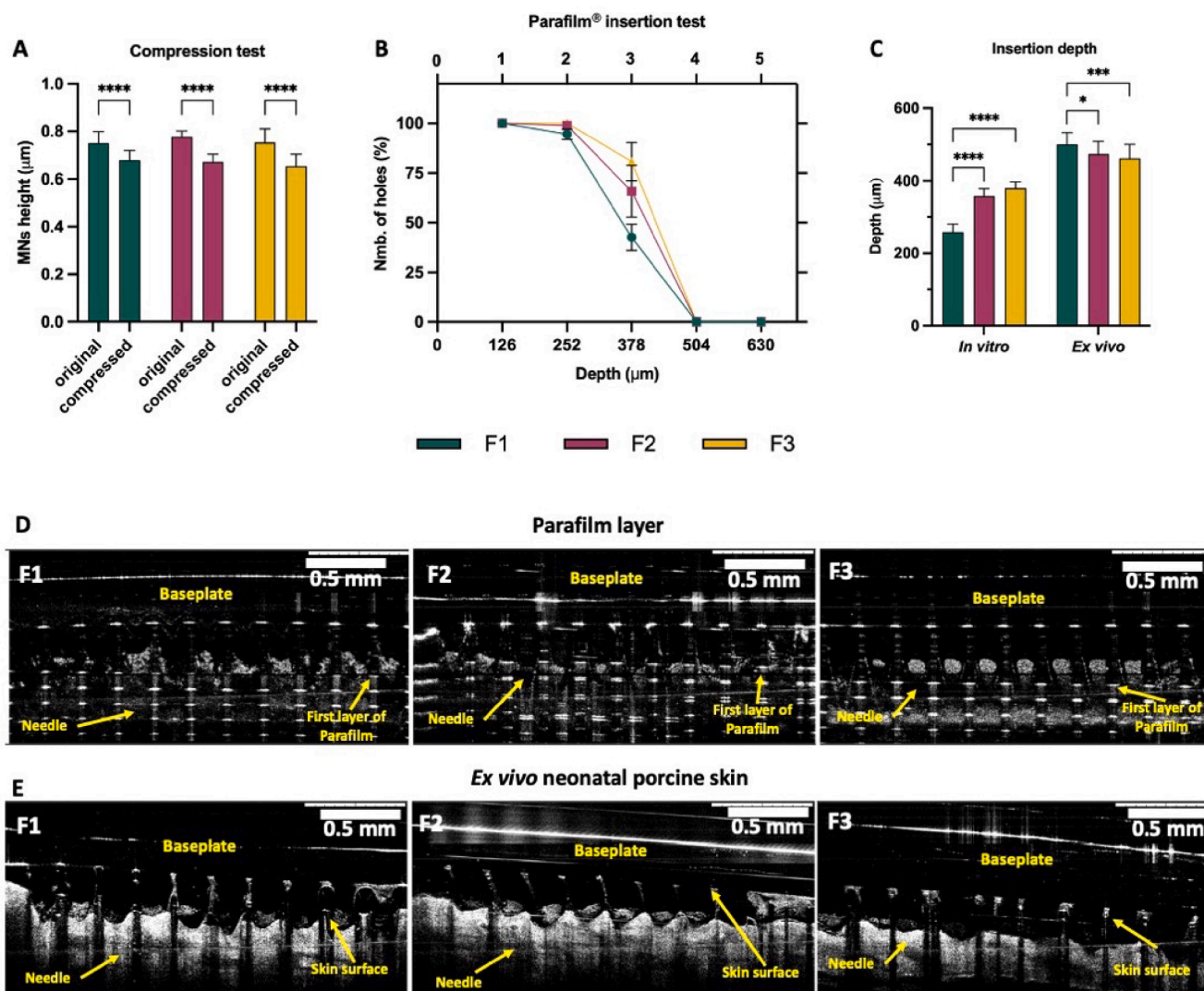
Fig. 11. (A) LipoRIF-DMNs height reduction following application of a force of 32 N (mean + SD, n = 25). (B) Percentage of holes generated per Parafilm® M layer upon the insertion of LipoRIF-DMNs (mean ± SD., n = 3). (C) Insertion depth LipoRIF-DMNs into Parafilm® M layer and ex vivo neonatal porcine skin as quantified from OCT images (means + SD., n = 20). OCT images of respective LipoRIF-DMNs formulation into (D) Parafilm® M layer and (E) ex vivo neonatal porcine skin.

of Parafilm®M were used as a validated *in vitro* skin simulant (Larrañeta et al., 2014). All the formulations were able to breach the Parafilm® stack up to the third layer, which is equal to ~ 378 μm, with the highest insertion for F3 (Fig. 11**B**) (F1 vs F2 $p < 0.0001$; F1 vs F3 $p < 0.0001$; F2 vs F3 $p = 0.001$). In comparison, *ex vivo* neonatal porcine skin was utilised to predict the *in vivo* insertion depth due to its similarities to human skin (Ranamukhaarachchi et al., 2016); insertion depth was recorded by OCT (Fig. 11**C, 11D, 11 E**). The results showed that all three formulations pierced the full-thickness porcine skin up to ~ 500 μm. F1 provided the greater *ex vivo* insertion (F1 vs. F2 $p < 0.05$; F1 vs. F3 $p < 0.001$; F2 vs. F3 $p = 0.48$). This insertion depth is promising for sub-epidermal infection treatment to be successful as pathogenic bacteria are typically present at a depth of 400–700 μm during skin infection (Anjani et al., 2022; Touitou et al., 1998).

The *ex vivo* dissolution profile of F1, F2 and F3 LipoRIF-DMNs was assessed in neonatal porcine skin, as presented in Fig. 12. Most tips disintegrated after 5 min from the skin insertion, with a complete dissolution detectable after 30 min. RIF appears deposited in the skin samples at the end of the test. F1 was selected as the leader formulation considering the highest RIF loading, the lower MNs height percentage reduction following the compression test and the deeper *ex vivo* insertion ability.

3.3.2. Evaluation of LipoRIF-DMNs

F1 LipoRIF-DMNs, from now on named LipoRIF-DMNs, were further evaluated in terms of morphology, *ex vivo* RIF intradermal delivery efficiency, stability, biocompatibility and antimicrobial properties. TEM micrographs (Fig. 13**C**) confirmed the liposome-like structure of the vesicles released by the DMNs platform SEM images (Fig. 13**A**) and multiphoton analysis (Fig. 13**B**) confirmed LipoRIF-DMNs had sharp tips and smooth baseplate; still, "bulges" were detected in the surface of the formulation and/or in the inner matrix. To better understand the nature of the bulges, a morphological investigation of the LipoRIF/polymer blend used to fabricate the LipoRIF DMNs array was performed. Optical microscopy showed a not-smooth surface, with bulges and round-shaped structures visible at SEM (Fig. 13**D-F**). Considering that fluorescence of bulges under multiphoton microscopy appears more intense than the rest of the DMNs system and assessing the crested surface of the cast LipoRIF/polymer blend, the most probable explanation is that bulges represent freeze-dried LipoRIF which aggregated during the LipoRIF/polymer mixing process to obtain the final blend. Indeed, no stabilising (surfactant) agents or electrically charged components influencing vesicle surface charge were added to the liposome composition resulting in aggregation phenomena being more likely to happen, particularly if subjected to high-energy homogenisation processes (Demartis et al., 2021). Nevertheless, the presence of "bulge" did not significantly affect the mechanical performance of the system; therefore, it was not considered a reason to exclude the formulation.

3.4. Skin deposition study of LipoRIF-DMNs

LipoRIF-DMNs were designed to target the epidermal and dermal skin layers aiming at local MRSA eradication in the management of SSTIs. Thus, transdermal systemic absorption of the active drug was intended to be avoided. The delivery performances of LipoRIF-DMNs in terms of intradermal deposition and transdermal absorption were evaluated and compared to LipoRIF dispersion. The dermatokinetic profiles of both formulations are reported in Fig. 14. It is evident from the results that, for the time tested, the intradermal delivery efficiency was much higher for LipoRIF-DMNs (~40 %) than LipoRIF dispersion (~5%), which instead provided a transdermal absorption. Based on the characteristics of the formulations that were tested, we observed vesicles that were approximately 220 nm in size in the case of LipoRIF dispersion. Additionally, both vesicles and aggregates of the vesicles (observed "bulges") were embedded in a polymeric matrix that was approximately 335 nm in size. In this scenario, once DMNs are inserted into the skin,

the polymer dissolves, releasing what is embedded in the polymer matrix. In the case of individual liposomes, they permeate through the dermis until they reach the target cells. In the case of liposome aggregates, it is likely that they gradually disaggregate once deposited into the dermis due to the presence of water (it is important to note that the water percentage in the dermis is about 70 % in healthy young adults) (Kaye et al., 2019). In this context, liposome-like vesicles naturally tend to avoid dry surroundings due to the presence of an aqueous core, and the driving force for permeation is the transdermal hydration gradient (Suaya et al., 2013). Once aggregates transform into smaller aggregates or single liposomes, they can more easily permeate through the skin until they interact with target cells, such as MRSA strains. The presence of LipoRIF in the skin could potentially enhance interactions with MRSA strains, thus facilitating the eradication of SSTIs (Suaya et al., 2013).

Concerning the topically applied LipoRIF dispersion, statistical analysis proved that the RIF amount definitively increased within the skin over time (RIF in the epidermis at 1 h vs RIF in the epidermis at 24 h $p < 0.01$; RIF dermis at 1 h vs RIF dermis at 24 h $p < 0.01$) and a transdermal absorption is evident at 24 h. Various mechanisms of liposome permeation have been described in literature, such as: (i) the process of liposome components enhancing penetration, (ii) vesicle adsorption to the *stratum corneum* or fusion with it, and (iii) penetration of intact vesicles into or through the skin (El Maghraby et al., 2006). Considering the size and not elastic properties of LipoRIF herein developed, the most probable mechanism is the initial adhesion onto the skin surface, with the adsorption to and/or fusion with the lipid matrix of SC, thereby releasing RIF and increasing its partitioning through the skin. First, the adsorption/fusion of LipoRIF with the SC helped RIF to overcome the SC barrier, naturally hampered by RIF's high molecular weight. Subsequently, RIF likely migrated from the outmost skin layer toward the acceptor medium due to RIF's proper balance between lipophilicity and pH-dependent solubility in aqueous media, guided by the transdermal hydration gradient driving force (Demartis et al., 2021; Demartis et al., 2022). Indeed, it is important to note that a molecule's lipophilicity is a key parameter affecting the ability to cross the SC barrier; still, water-solubility is essential to favour the proper migration through the water-rich dermis environment (Iqbal et al., 2018; Zoabi et al., 2021). This explanation is further supported by the micrographs acquired using multiphoton microscopy (Fig. 14**A**), where the progressive reduction of fluorescence intensity is visible. In the case of LipoRIF-DMNs, the considerable RIF deposition in the skin is a straightforward consequence of using polymer MNs. Polymeric DMNs pierced the SC barrier, dissolved and released LipoRIF vesicles directly into the skin. Herein, the SC-LipoRIF interaction did not occur; thus, the fusion/adsorption processes of the vesicles were minimised and LipoRIF structural integrity could be maintained (Demartis et al., 2022; Yang et al., 2019). Statistical analysis and data observations suggest the total RIF amount in the skin and the partitioning between the epidermis and dermis did not change over time ($p > 0.05$), resulting in a static-like dosage form. The use of polymer clearly affects the external surface of the liposome, as can be observed here from the size and as previously reported by the same author (Suaya et al., 2013). Using "virgin" liposomes resulted in about 15 % transdermal absorption. The size is indeed too large to facilitate proper transdermal delivery (blood capillaries allow the entry of particles smaller than 10 nm, and lymph nodes range between 10 and 150 nm). However, the composition of the bilayer is similar to that of human cells, which promotes interaction phenomena with cells and blood components. On the contrary, the presence of hydrophilic polymer on the outer surface of the liposome bilayer, along with the larger size (335 nm), likely hinders this interaction by making liposomes sterically stable and promoting deposition in the dermal layer (Zimmerli and Sendi, 2019). This phenomenon resulted in a significant intradermal deposition of RIF. The presence of the LipoRIF in the skin may enhance the interaction with MRSA strains, favouring the eradication of SSTIs (Singh et al., 2014; Gonzalez Gomez and Hosseinidoust, 2020).
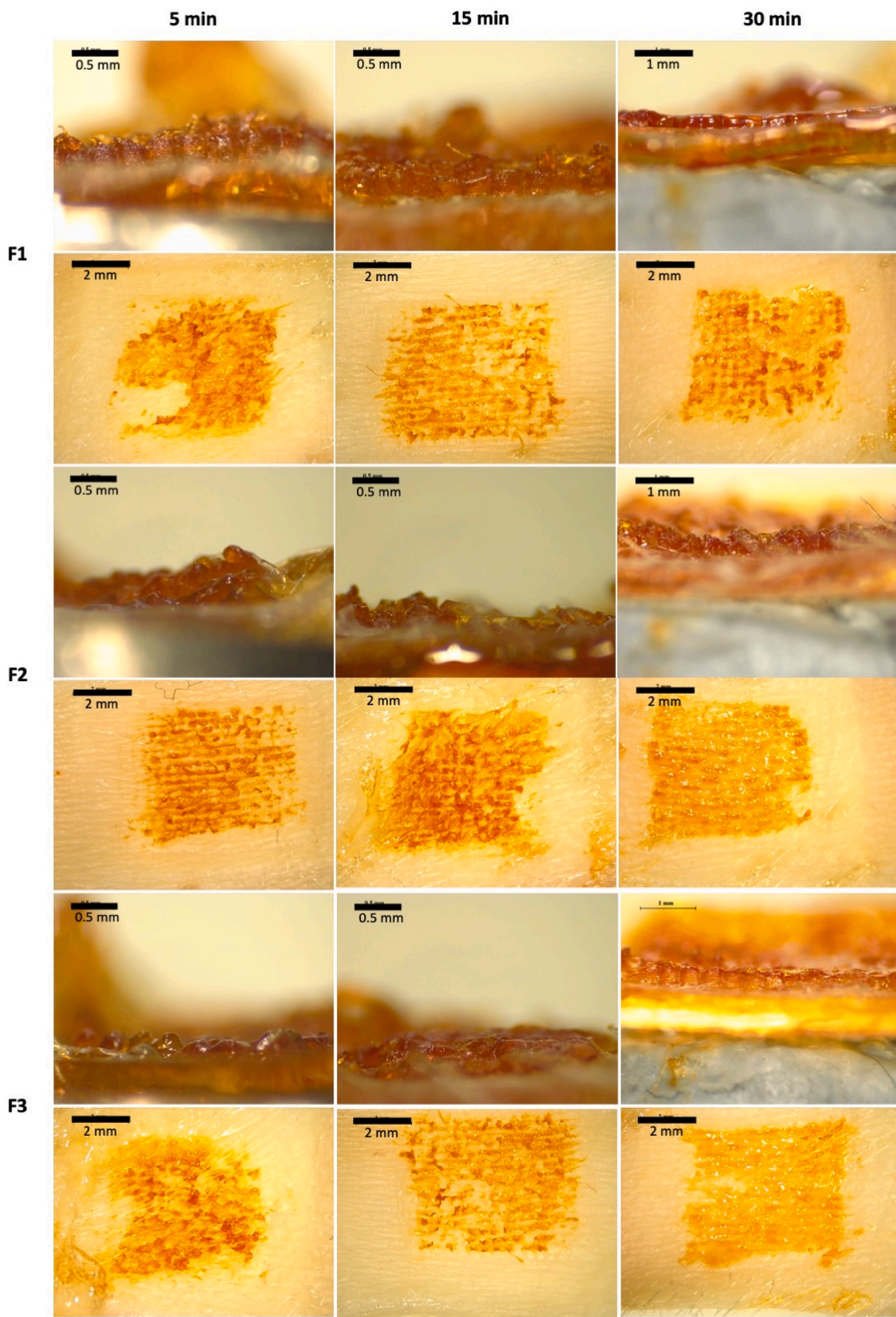
Fig. 12. Images of LipoRIF-DMNs formulations dissolving in the skin at 5 min, 15 min and 30 min acquired by optical microscopy.
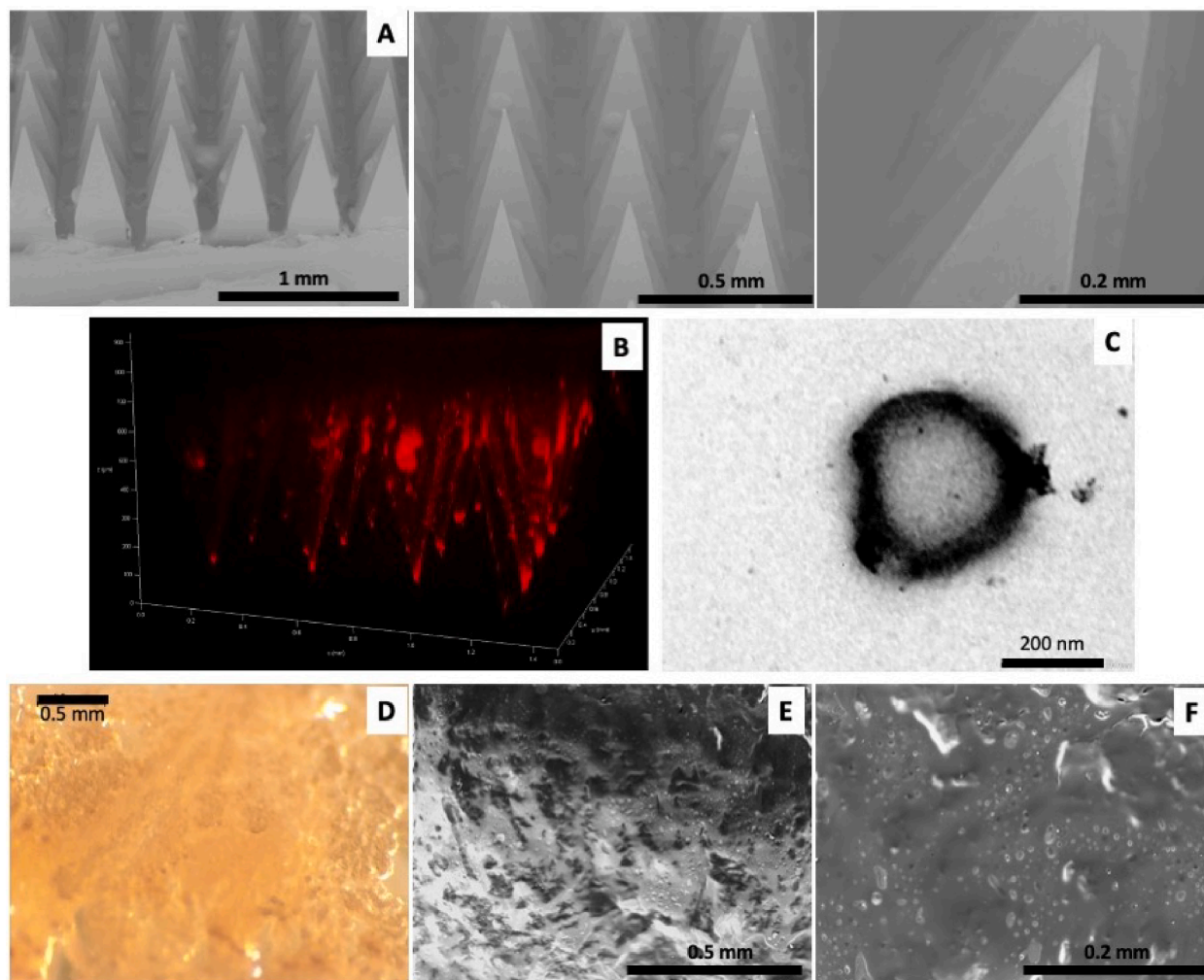
Fig. 13. Images of LipoRIF-DMNs acquired at (A) SEM, (B) multiphoton microscopy. TEM micrograph of redispersed LipoRIF from LipoRIF-DMNs (C). Film observed at (D) optical microscopy and (E,F) SEM.

3.5. Stability studies of DMNs

Similar to the LipoRIF formulation, short-term and accelerated stability study were also carried out for LipoRIF-DMNs to ensure that the DMNs still have adequate mechanical strength and no chemical degradation upon storage. The percentage of needle height reduction of DMNs following storage under different conditions is presented in Fig. 15**A**. We observed no significant change in mechanical properties ($p > 0.05$) of the DMNs over the study period. Furthermore, as shown in Fig. 15**B**, no significant difference was found for drug content per DMN throughout the storage period ($p > 0.05$), implying that incorporating LipoRIF and DMN can prevent drug degradation.

3.6. Biocompatibility study

The biocompatibility of ULipo-DMNs and LipoRIF-DMNs with fibroblast cells was assessed by conducting an MTT assay to examine any potential cytotoxic effects of the formulations. As presented in Fig. 16 **(A),** both ULipo-DMNs and LipoRIF-DMNs caused only a minor decrease in cell viability (91.64 % and 91.25 %, respectively) in comparison to the control group (plate fibroblast cell culture). Statistical analysis demonstrated a significant difference between the control cells and LIP ($p < 0.001$) or LipoRIF-DMNs ($p < 0.001$), indicating that RIF influenced the cell viability to some extent. Nevertheless, according to previous studies that described cytotoxicity classifications (Li et al., 2015), the

ISO 10993–5 guidelines (Charcosset et al., 2015), and a 5-point grading scale as previously reported (Utomo et al., 2022), ULipo-DMNs and LipoRIF-DMNs were designated as Grade 1, indicating no cytotoxicity and no observable toxicity towards fibroblast cells. This finding is in line with Gruppuso *et al.*'s observations that RIF and its formulations did not cause any noticeable reduction in cell viability in fibroblast cells (Gruppuso et al., 2022).

Moreover, to assess the effect of the formulation and excipient on the growth of healthy cells, the PicoGreen assay was conducted after 72 h of exposure. The results depicted in Fig. 16**(B)** revealed that the proliferation of fibroblast cells was not influenced by ULipo-DMNs and LipoRIF-DMNs. In addition, the absence of red fluorescence in cells treated with ULipo-DMNs and LipoRIF-DMNs following Calcein/Ethidium Homodimer-1 staining was presented in Fig. 16**(C)**, indicating no extracellular release of nucleic acid from dead cells with damaged plasma membranes. It is worth noting that distinct optical variations in cell morphology were observed in the groups treated with DMNs (both ULipo and LipoRIF) compared to the control group due to the altered cell adhesion brought about by changes in cell morphology after exposure to biomaterials, aligning with previously published research (Versaevel et al., 2012; Khalili and Ahmad, 2015; Farias et al., 2018). Overall, the findings from Fig. 16 suggest that delivering LipoRIF *via* DMNs may not cause any considerable toxicity to the skin as it does not compromise the viability or plasma membrane integrity of the cells.
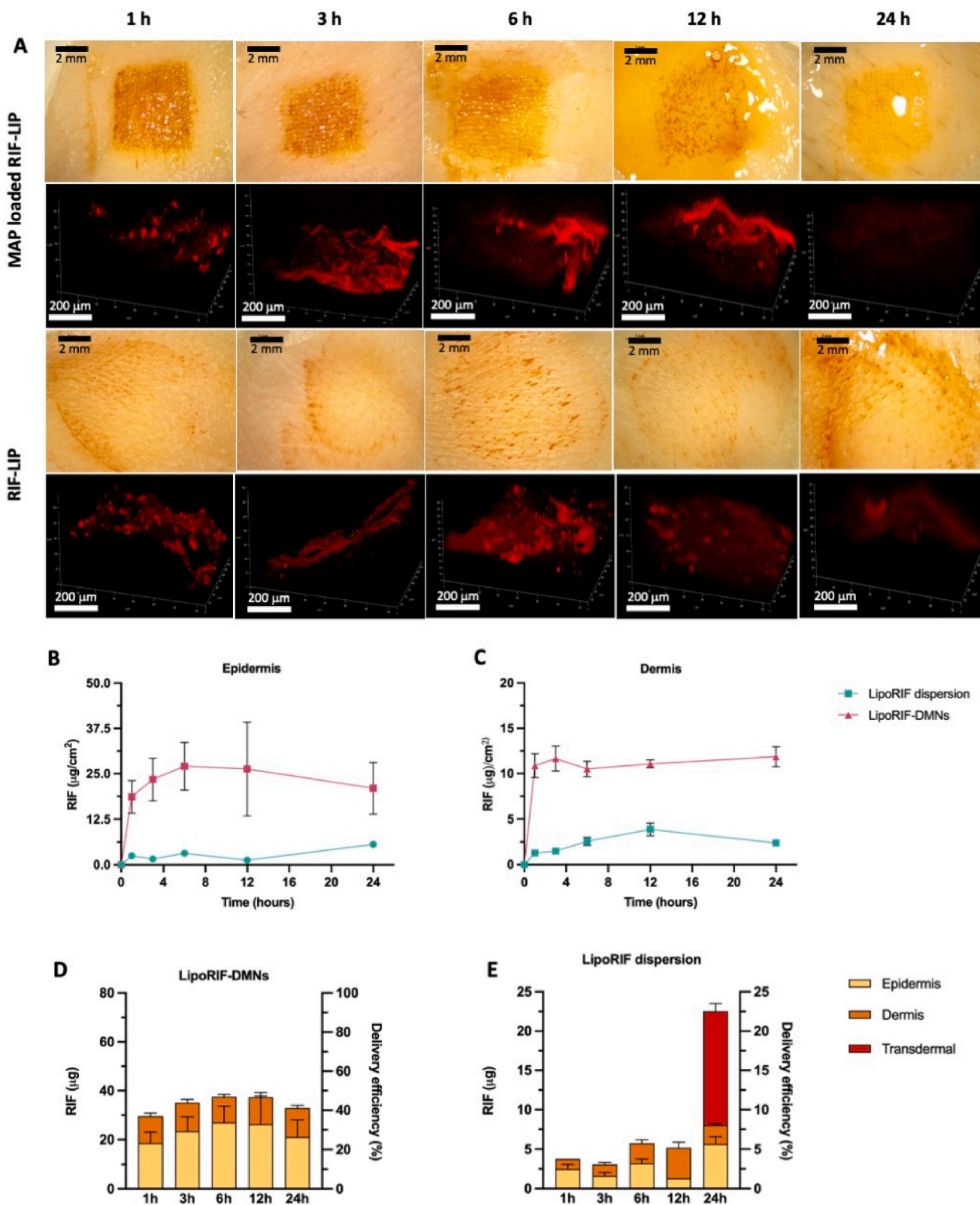
Fig. 14. (A) Micrographs of neonatal porcine skin samples at the end of 24-hour permeation study acquired by digital light microscopy and multiphoton microscopy. Amount of RIF extracted from (B) epidermis, (C) dermis of excised neonatal porcine skin (means ± SEM, n = 4). Total delivery and distribution of RIF following application (D) LipoRIF-DMN and (E) LipoRIF dispersion (means + SEM, n = 4).
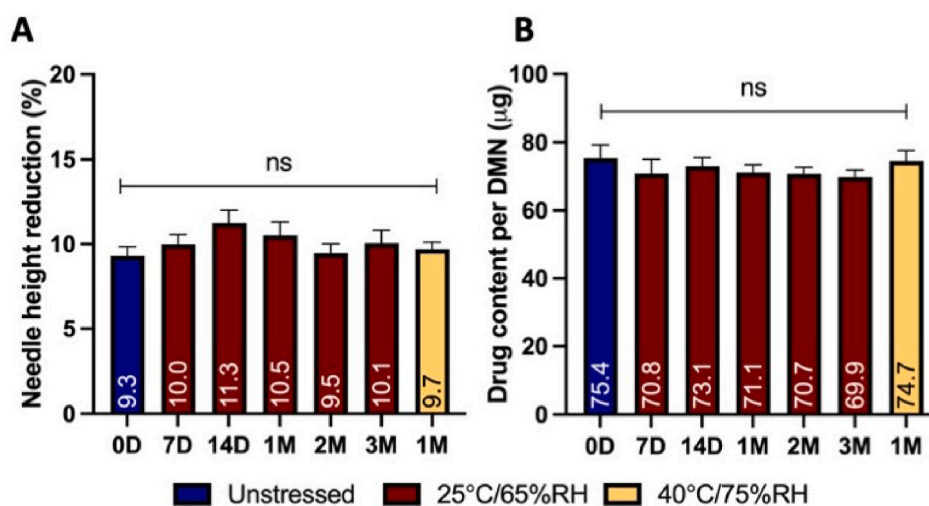
Fig. 15. (A) Percentage of needle height reduction after compression and (B) drug content of RIF-LIP loaded MAP after storage at different conditions (means + SD, n = 4). D = day, M = month.
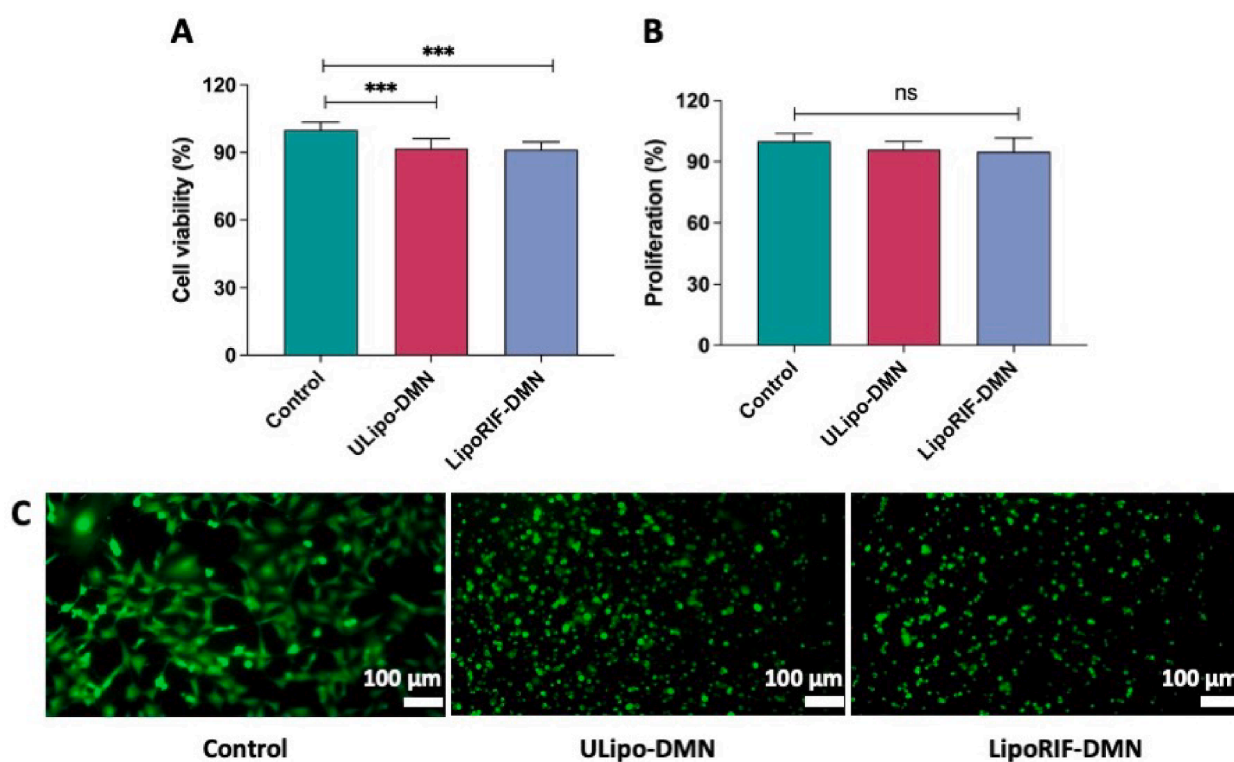

Fig. 16. Biocompatibility of ULipo-DMNs and LipoRIF-DMNs on fibroblast. (A) Percentage of viable cells after a culture period of 72 h (means + SD, n = 6). (B) Total DNA content of cells on control, ULipo-DMNs and LipoRIF-DMNs (means + SD, n = 6). (C) Results of the live/dead staining of fibroblastic cells on control (plate cells culture), ULipo-DMNs and LipoRIF-DMNs, where green represents live cells and red represents dead cells.

3.7. In vitro antibacterial activity of LipoRIF-DMNs

A disk diffusion experiment was performed to evaluate the antimicrobial effect of the LipoRIF-DMNs on a bacterial culture of MRSA. The results of the disk diffusion test are shown in Fig. 17. LipoRIF-DMNs samples showed a clear zone of inhibition of approximately 45 mm in diameter in MRSA plates. However, as LipoRIF dispersions were delivered *via* dissolving MN technology, the inhibition zones presented irregular forms (**Figure S2, supplementary data**). Additionally, to evaluate that only the loaded RIF caused the zone of inhibition, blank DMNs and ULipo-DMNs were also tested for antimicrobial effect on a bacterial culture of MRSA. Although a clearer area was observed in the MH agar plates where these samples were placed, this was not a zone of inhibition, and it only shows the polymer was dissolved. Thus, these outcomes demonstrate that neither the polymers used for DMN manufacture nor the phospholipid used for liposome preparation provide any meaningful antimicrobial effect against MRSA. Similar results against *Bacteroides fragilis*, which is also associated with skin and soft-tissue infections (SSTIs), have already been reported by using metronidazole nanosuspension (NS)-loaded dissolving MNs (Anjani et al., 2022). In line with this, amphotericin B microparticles-loaded DMNs also showed their potential for treating cutaneous fungal infections (Peng et al., 2021).
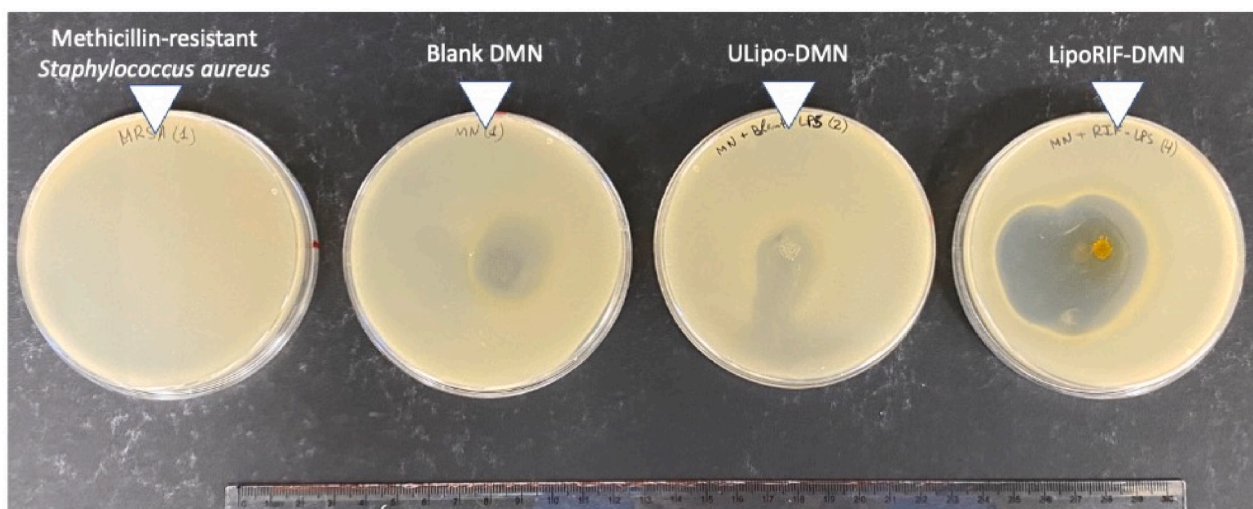
Fig. 17. Representative image showing the inhibition obtained for MRSA in MH agar using LipoRIF-DMNs (n = 5). The scale unit is in centimetres.

MRSA is a pathogen that can be transmitted in both healthcare and community settings, leading to SSTIs in the community (Pulido Pérez et al., 2014), reaching incidence rates of about 19.8 per 100,000 people (Mascitti et al., 2010). Moreover, patients suffering from severe or antibiotic-resistant SSTIs may need hospitalization (Bassetti et al., 2014). Therefore, according to this information and the results obtained in our work, DMN technology may be a very promising strategy for the treatment of SSTIs caused by MRSA.

4. Conclusions

The current work presented the development and characterisation of DMNs as liposomal RIF intradermal delivery systems in eradicating MRSA-induced STTIs. In this frame, DMNs may play a crucial role in combating MDR as they painlessly pierce the skin releasing a precise dosage of active cargo directly to the target site. The obtained LipoRIF formulation was nanosized, stable and highly efficient in encapsulating RIF and was subsequently converted in the DMNs platform, varying some formulation and process parameters. The selected LipoRIF-DMNs formulation proved strong enough to efficiently pierce the skin and rapidly dissolved in the tissue fluid, releasing LipoRIF, which were initially deposited into the site typically affected by superficial SSTIs. Notably, DMNs significantly increased LipoRIF deposition in the skin compared to the LipoRIF dispersion, which promoted undesired RIF transdermal absorption instead. Finally, LipoRIF-DMNs demonstrated no measurable cytotoxicity to healthy cells; conversely, the MRSA antimicrobial activity was evident. This investigation proved the reliability of relaunching the long-standing drug RIF to eradicate SSTIs assisted by a pharmaceutical technology innovation to limit RIF disadvantages. The current research represents the first step of the study. Further tests will be carried out to better elucidate the potential of the newly developed RIF delivery system, including a long-term *in vivo* dermatokinetic study.

5. Ethical Approval Statement

NA.

6. Informed Consent Statement

NA.

CRediT authorship contribution statement

Qonita Kurnia Anjani: Conceptualization, Methodology, Visualization, Investigation, Validation, Formal analysis, Data curation, Writing – original draft, Writing – review & editing. **Anjali K. Pandya:** Conceptualization, Investigation, Writing – original draft. **Sara Demartis:** Conceptualization, Visualization, Writing – original draft, Writing – review & editing. **Juan Domínguez-Robles:** Methodology, Investigation. **Natalia Moreno-Castellanos:** Methodology, Investigation. **Huanhuan Li:** Methodology, Investigation. **Elisabetta Gavini:** Writing – review & editing, Supervision. **Vandana B. Patravale:** Writing – review & editing, Supervision. **Ryan F. Donnelly:** Resources, Writing – review & editing, Supervision, Funding acquisition.

Declaration of Competing Interest

The authors declare that they have no known competing financial interests or personal relationships that could have appeared to influence the work reported in this paper.

Data availability

Data will be made available on request.

Appendix A. Supplementary data

Supplementary data to this article can be found online at https://doi.org/10.1016/j.ijpharm.2023.123446.

References

Agrawal, S., Panchagnula, R., 2004. Dissolution test as a surrogate for quality evaluation of rifampicin containing fixed dose combination formulations. Int. J. Pharm. 287, 97–112. https://doi.org/10.1016/J.IJPHARM.2004.09.005.

Alberts, B., Johnson, A., Lewis, J., Raff, M., Roberts, K., Walter, P., Cells, T., Proteins, M. H.C., 2008 (accessed April 27, 2023). Mol Biol Cell. 1569–1588. http://www.ncbi.nlm.nih.gov/books/NBK26926/.

Altuntaş, E., Tekko, I.A., Vora, L.K., Kumar, N., Brodsky, R., Chevallier, O., McAlister, E., Kurnia Anjani, Q., McCarthy, H.O., Donnelly, R.F., 2022. Nestorone nanosuspension-loaded dissolving microneedles array patch: A promising novel approach for "on-demand" hormonal female-controlled peritcoital contraception. Int. J. Pharm. 614, 121422 https://doi.org/10.1016/J.IJPHARM.2021.121422.

Alves, R., Reis, T.V.D.S., Da Silva, L.C.C., Storpírtis, S., Mercuri, L.P., Matos, J.D.R., 2010. Thermal behavior and decomposition kinetics of rifampicin polymorphs under isothermal and non-isothermal conditions, Brazilian. J. Pharm. Sci. 46, 343–351. https://doi.org/10.1590/S1984-82502010000200022.

Anjani, Q.K., Domínguez-Robles, J., Utomo, E., Font, M., Martínez-Ohárriz, M.C., Permana, A.D., Cárcamo-Martínez, Á., Larrañeta, E., Donnelly, R.F., 2021. Inclusion Complexes of Rifampicin with Native and Derivatized Cyclodextrins: In Silico Modeling, Formulation, and Characterization, Pharmaceuticals (Basel). 15. https://doi.org/10.3390/PH15010020.

Anjani, Q.K., Permana, A.D., Cárcamo-Martínez, Á., Domínguez-Robles, J., Tekko, I.A., Larrañeta, E., Vora, L.K., Ramadon, D., Donnelly, R.F., 2021. Versatility of hydrogel-forming microneedles in in vitro transdermal delivery of tuberculosis drugs. Eur. J. Pharm. Biopharm. 294–312, 294–312. https://doi.org/10.1016/j.ejpb.2020.12.003.

Anjani, Q.K., Bin Sabri, A.H., Utomo, E., Domínguez-Robles, J., Donnelly, R.F., 2022. Elucidating the Impact of Surfactants on the Performance of Dissolving Microneedle Array Patches. acs.molpharmaceut.1c00988 Mol Pharm.. https://doi.org/10.1021/ACS.MOLPHARMACEUT.1C00988.

Anjani, Q.K., Hidayat, A., Sabri, B., Moreno-Castellanos, N., Utomo, E., Cárcamo-Martínez, Á., Domínguez-Robles, J., Ahmadi, L., Wardoyo, H., Donnelly, R.F., 2022. Soluplus®-based dissolving microarray patches loaded with colchicine: towards a minimally invasive treatment and management of gout. Biomater. Sci. https://doi.org/10.1039/D2BM01068B.

Anjani, Q.K., Bin Sabri, A.H., McGuckin, M.B., Li, H., Hamid, K.A., Donnelly, R.F., 2022. In Vitro Permeation Studies on Carvedilol Containing Dissolving Microarray Patches Quantified Using a Rapid and Simple HPLC-UV Analytical Method. AAPS PharmSciTech. 23, 1–13. https://doi.org/10.1208/S12249-022-02422-6/FIGURES/4.

Anjani, Q.K., Bin Sabri, A.H., Domínguez-Robles, J., Moreno-Castellanos, N., Utomo, E., Wardoyo, L.A.H., Larrañeta, E., Donnelly, R.F., 2022. Metronidazole nanosuspension loaded dissolving microarray patches: An engineered composite pharmaceutical system for the treatment of skin and soft tissue infection. Biomater. Adv. 140, 213073 https://doi.org/10.1016/J.BIOADV.2022.213073.

Anjani, Q.K., Bin Sabri, A.H., Hamid, K.A., Moreno-Castellanos, N., Li, H., Donnelly, R.F., 2023. Tip loaded cyclodextrin-carvedilol complexes microarray patches. Carbohydr. Polym. 320, 121194. 10.1016/j.carbpol.2023.121194.

Anjani, Q.K., Volpe-Zanutto, F., Hamid, K.A., Bin Sabri, A.H., Moreno-Castellano, N., Gaitán, X.A., Calit, J., Bargieri, D.Y., Donnelly, R.F., 2023. Primaquine and chloroquine nano-sized solid dispersion-loaded dissolving microarray patches for the improved treatment of malaria caused by Plasmodium vivax. J. Control. Release 361, 385–401. https://doi.org/10.1016/J.JCONREL.2023.08.009.

Anjani, Q.K., Bin Sabri, A.H., Hutton, A.J., Cárcamo-Martínez, Á., Wardoyo, L.A.H., Mansoor, A.Z., Donnelly, R.F., 2023. Microarray patches for managing infections at a global scale. J. Control. Release 359, 97–115. 10.1016/j.jconrel.2023.05.038.

Anjani, Q.K., Cárcamo-Martínez, Á., Wardoyo, L.A.H., Moreno-Castellanos, N., Bin Sabri, A.H., Larrañeta, E., Donnelly, R.F., 2023. MAP-box: a novel, low-cost and easy-to-fabricate 3D-printed box for the storage and transportation of dissolving microneedle array patches, Drug Deliv. Transl Res. https://doi.org/10.1007/s13346-023-01393-w.

Bassetti, M., Baguneid, M., Bouza, E., Dryden, M., Nathwani, D., Wilcox, M., 2014. European perspective and update on the management of complicated skin and soft tissue infections due to methicillin-resistant Staphylococcus aureus after more than 10 years of experience with linezolid. Clin. Microbiol. Infect. 20, 3–18. https://doi.org/10.1111/1469-0691.12463.

Bin Sabri, A.H., Anjani, Q.K., Donnelly, R.F., Hidayat Bin Sabri, A., Kurnia Anjani, Q., Donnelly, R.F., 2021. Synthesis and characterization of sorbitol laced hydrogel-forming microneedles for therapeutic drug monitoring. Int. J. Pharm. 607, 121049.

Bin Sabri, A.H., Anjani, Q.K., Gurnani, P., Domínguez-Robles, J., Moreno-Castellanos, N., Zhao, L., Hutton, A.R.J., Donnelly, R.F., 2023. Fabrication and characterisation of poly(sulfonated) and poly(sulfonic acid) dissolving microneedles for delivery of antibiotic and antifungal agents. Int. J. Pharm. 644, 123292 https://doi.org/10.1016/J.IJPHARM.2023.123292.

Cárcamo-Martínez, Á., Anjani, Q.K., Permana, A.D., Cordeiro, A.S., Larrañeta, E., Donnelly, R.F., 2020. Coated polymeric needles for rapid and deep intradermal delivery. Int J Pharm X. 2, 100048 https://doi.org/10.1016/j.ijpx.2020.100048.

Cevc, G., 1996. Transfersomes, liposomes and other lipid suspensions on the skin: permeation enhancement, vesicle penetration, and transdermal drug delivery. Crit. Rev. Ther. Drug Carrier Syst. 13, 257–388. https://doi.org/10.1615/CRITREVTHERDRUGCARRIERSYST.V13.I3-4.30.

Charcosset, C., Juban, A., Valour, J.P., Urbaniak, S., Fessi, H., 2015. Preparation of liposomes at large scale using the ethanol injection method: Effect of scale-up and injection devices. Chem. Eng. Res. Des. 94, 508–515. https://doi.org/10.1016/J.CHERD.2014.09.008.

Coulman, S.A., Anstey, A., Gateley, C., Morrissey, A., McLoughlin, P., Allender, C., Birchall, J.C., 2009. Microneedle mediated delivery of nanoparticles into human skin. Int. J. Pharm. 366, 190–200. https://doi.org/10.1016/J.IJPHARM.2008.08.040.

Demartis, S., Rassu, G., Murgia, S., Casula, L., Giunchedi, P., Gavini, E., 2021. Improving Dermal Delivery of Rose Bengal by Deformable Lipid Nanovesicles for Topical Treatment of Melanoma. Mol. Pharm. 18, 4046–4057. https://doi.org/10.1021/ACS.MOLPHARMACEUT.1C00468/SUPPL_FILE/MP1C00468_SI_001.PDF.

Demartis, S., Anjani, Q.K., Volpe-Zanutto, F., Paredes, A.J., Jahan, S.A., Vora, L.K., Donnelly, R.F., Gavini, E., 2022. Trilayer dissolving polymeric microneedle array loading Rose Bengal transfersomes as a novel adjuvant in early-stage cutaneous melanoma management. Int. J. Pharm. 627, 122217 https://doi.org/10.1016/J.IJPHARM.2022.122217.

Dhoble, S., Patravale, V., 2019. Development of anti-angiogenic erlotinib liposomal formulation for pulmonary hypertension: a QbD approach. Drug Deliv Transl. Res. 9, 980–996. https://doi.org/10.1007/S13346-019-00641-2/FIGURES/13.

El Maghraby, G.M.M., Williams, A.C., Barry, B.W., 2006. Can drug-bearing liposomes penetrate intact skin? J. Pharm. Pharmacol. 58, 415–429. https://doi.org/10.1211/JPP.58.4.0001.

El-Naggar, M.M., El-Nabarawi, M.A., Teaima, M.H., Hassan, M., Hamed, M.I.A., Elrashedy, A.A., Albash, R., 2023. Integration of terpesomes loaded Levocetrizine dihydrochloride gel as a repurposed cure for Methicillin-Resistant Staphylococcus aureus (MRSA)-Induced skin infection; D-optimal optimization, ex-vivo, in-silico, and in-vivo studies. Int. J. Pharm. 633 https://doi.org/10.1016/J.IJPHARM.2023.122621.

El-Nesr, O.H., Yahiya, S.A., El-Gazayerly, O.N., 2010. Effect of formulation design and freeze-drying on properties of fluconazole multilamellar liposomes. Saudi Pharm J. 18, 217–224. https://doi.org/10.1016/J.JSPS.2010.07.003.

Faizi, H.S., Vora, L.K., Nasiri, M.I., Wu, Y., Mishra, D., Anjani, Q.K., Paredes, A.J., Thakur, R.R.S., Minhas, M.U., Donnelly, R.F., 2022. Deferasirox Nanosuspension Loaded Dissolving Microneedles for Intradermal Delivery. Pharmaceutics 14, 2817. https://doi.org/10.3390/PHARMACEUTICS14122817.

Farias, C., Lyman, R., Hemingway, C., Chau, H., Mahacek, A., Bouzos, E., Mobed-Miremadi, M., 2018. Three-Dimensional (3D) Printed Microneedles for Microencapsulated Cell Extrusion. Bioengineering 5, 59. https://doi.org/10.3390/BIOENGINEERING5030059.

Ferreira, M., Ogren, M., Dias, J.N.R., Silva, M., Gil, S., Tavares, L., Aires-Da-silva, F., Gaspar, M.M., Aguiar, S.I., 2021. Liposomes as Antibiotic Delivery Systems: A Promising Nanotechnological Strategy against Antimicrobial Resistance. Molecules 26. https://doi.org/10.3390/MOLECULES26072047.

Forrest, G.N., Tamura, K., 2010. Rifampin Combination Therapy for Nonmycobacterial Infections. Clin. Microbiol. Rev. 23, 14. https://doi.org/10.1128/CMR.00034-09.

Ghodake, V., Vishwakarma, J., Vavilala, S.L., Patravale, V., 2020. Cefoperazone sodium liposomal formulation to mitigate P. aeruginosa biofilm in Cystic fibrosis infection: A QbD approach. Int. J. Pharm. 587, 119696 https://doi.org/10.1016/J.IJPHARM.2020.119696.

Giacobbe, D.R., Dettori, S., Corcione, S., Vena, A., Sepulcri, C., Maraolo, A.E., De Rosa, F. G., Bassetti, M., 2022. Emerging Treatment Options for Acute Bacterial Skin and Skin Structure Infections and Bloodstream Infections Caused by Staphylococcus aureus: A Comprehensive Review of the Evidence. Infect Drug Resist. 15, 2137–2157. https://doi.org/10.2147/IDR.S318322.

Gonzalez Gomez, A., Hosseinidoust, Z., 2020. Liposomes for Antibiotic Encapsulation and Delivery, ACS. Infect. Dis. 6, 896–908. https://doi.org/10.1021/ACSINFECDIS.9B00357/ASSET/IMAGES/LARGE/ID9B00357_0009.JPEG.

González-González, O., Ramirez, I.O., Ramirez, B.I., O'Connell, P., Ballesteros, M.P., Torrado, J.J., Serrano, D.R., 2022. Drug Stability: ICH versus Accelerated Predictive Stability Studies. Pharmaceutics. 14, 2324. https://doi.org/10.3390/PHARMACEUTICS14112324.

Gouda, A., Sakr, O.S., Nasr, M., Sammour, O., 2021. Ethanol injection technique for liposomes formulation: An insight into development, influencing factors, challenges and applications. J Drug Deliv Sci Technol. 61, 102174 https://doi.org/10.1016/J.JDDST.2020.102174.

Gruppuso, M., Guagnini, B., Musciacchio, L., Bellemo, F., Turco, G., Porrelli, D., 2022. Tuning the Drug Release from Antibacterial Polycaprolactone/Rifampicin-Based Core-Shell Electrospun Membranes: A Proof of Concept. ACS Appl. Mater. Interfaces 14, 27599–27612. https://doi.org/10.1021/ACSAMI.2C04849/ASSET/IMAGES/LARGE/AM2C04849_0010.JPEG.

Guillot, A.J., Cordeiro, A.S., Donnelly, R.F., Montesinos, M.C., Garrigues, T.M., Melero, A., 2020. Microneedle-Based Delivery: An Overview of Current Applications and Trends. Pharmaceutics. 12, 1–28. https://doi.org/10.3390/PHARMACEUTICS12060569.

Hindy, J.R., Haddad, S.F., Kanj, S.S., 2022. New drugs for methicillin-resistant Staphylococcus aureus skin and soft tissue infections. Curr. Opin. Infect. Dis. 35, 112–119. https://doi.org/10.1097/QCO.0000000000000800.

Huang, C., Gou, K., Yue, X., Zhao, S., Zeng, R., Qu, Y., Zhang, C., 2022. A novel hyaluronic acid-based dissolving microneedle patch loaded with ginsenoside Rg3 liposome for effectively alleviate psoriasis. Mater. Des. 224, 111363 https://doi.org/10.1016/J.MATDES.2022.111363.

Hulme, J., 2022. Application of Nanomaterials in the Prevention, Detection, and Treatment of Methicillin-Resistant Staphylococcus aureus (MRSA). Pharmaceutics. 14 https://doi.org/10.3390/PHARMACEUTICS14040805.

Iqbal, B., Ali, J., Baboota, S., 2018. Recent advances and development in epidermal and dermal drug deposition enhancement technology. Int. J. Dermatol. 57, 646–660. https://doi.org/10.1111/IJD.13902.

Israelachvili, J.N., Mitchell, D.J., Ninham, B.W., 1976. Theory of self-assembly of hydrocarbon amphiphiles into micelles and bilayers. J. Chem. Soc., Faraday Trans. 2: Mol Chem. Phys. 72, 1525–1568. https://doi.org/10.1039/F29767201525.

Jamaledin, R., Yiu, C.K.Y., Zare, E.N., Niu, L.N., Vecchione, R., Chen, G., Gu, Z., Tay, F. R., Makvandi, P., 2020. Advances in Antimicrobial Microneedle Patches for Combating Infections. Adv. Mater. 32, 2002129. https://doi.org/10.1002/ADMA.202002129.

Kaye, K.S., Petty, L.A., Shorr, A.F., Zilberberg, M.D., 2019. Current Epidemiology, Etiology, and Burden of Acute Skin Infections in the United States. Clin. Infect. Dis. 68, S193. https://doi.org/10.1093/CID/CIZ002.

Khalili, A.A., Ahmad, M.R., 2015. A Review of Cell Adhesion Studies for Biomedical and Biological Applications. Int. J. Mol. Sci. 16, 18149–18184. https://doi.org/10.3390/IJMS160818149.

Kim, J., Kim, B.E., Berdyshev, E., Bronova, I., Bin, L., Bae, J., Kim, S., Kim, H.Y., Lee, U. H., Kim, M.S., Kim, H., Lee, J., Hall, C.F., Hui-Beckman, J., Chang, Y., Bronoff, A.S.,

Hwang, D., Lee, H.Y., Goleva, E., Ahn, K., Leung, D.Y.M., 2023. Staphylococcus aureus causes aberrant epidermal lipid composition and skin barrier dysfunction. Allergy 00, 1–15. https://doi.org/10.1111/ALL.15640.

Larrañeta, E., Moore, J., Vicente-Pérez, E.M., González-Vázquez, P., Lutton, R., Woolfson, A.D., Donnelly, R.F., 2014. A proposed model membrane and test method for microneedle insertion studies. Int. J. Pharm. 472, 65–73. https://doi.org/10.1016/j.ijpharm.2014.05.042.

Li, R.Y., Liu, Z.G., Liu, H.Q., Chen, L., Liu, J.F., Pan, Y.H., 2015. Evaluation of biocompatibility and toxicity of biodegradable poly (DL-lactic acid) films. Am J Transl Res. 7, 1357. /pmc/articles/PMC4568792/ (accessed April 27, 2023).

Liu, J., Zheng, A., Peng, B., Xu, Y., Zhang, N., 2021. Size-Dependent Absorption through Stratum Corneum by Drug-Loaded Liposomes. Pharm. Res. 38, 1429–1437. https://doi.org/10.1007/S11095-021-03079-9.

Makabenta, J.M.V., Nabawy, A., Li, C.H., Schmidt-Malan, S., Patel, R., Rotello, V.M., 2020. Nanomaterial-based therapeutics for antibiotic-resistant bacterial infections. Nature Rev. Microbiol. 19, 23–36. https://doi.org/10.1038/s41579-020-0420-1.

Malaekeh-Nikouei, B., Fazly Bazzaz, B.S., Mirhadi, E., Tajani, A.S., Khameneh, B., 2020. The role of nanotechnology in combating biofilm-based antibiotic resistance. J Drug Deliv Sci Technol. 60, 101880 https://doi.org/10.1016/J.JDDST.2020.101880.

Mascitti, K.B., Gerber, J.S., Zaoutis, T.E., Barton, T.D., Lautenbach, E., 2010. Preferred treatment and prevention strategies for recurrent community-associated methicillin-resistant Staphylococcus aureus skin and soft-tissue infections: A survey of adult and pediatric providers. Am. J. Infect. Control 38, 324–328. https://doi.org/10.1016/J.AJIC.2009.11.007.

Nandhini, P., Kumar, P., Mickymaray, S., Alothaim, A.S., Somasundaram, J., Rajan, M., 2022. Recent Developments in Methicillin-Resistant Staphylococcus aureus (MRSA) Treatment: A Review. Antibiotics (basel). 11 https://doi.org/10.3390/ANTIBIOTICS11050606.

Obinu, A., Porcu, E.P., Piras, S., Ibba, R., Carta, A., Molicotti, P., Migheli, R., Dalpiaz, A., Ferraro, L., Rassu, G., Gavini, E., Giunchedi, P., 2020. Solid Lipid Nanoparticles as Formulative Strategy to Increase Oral Permeation of a Molecule Active in Multidrug-Resistant Tuberculosis Management. Pharmaceutics 12, 1132. https://doi.org/10.3390/PHARMACEUTICS12121132.

Opatha, S.A.T., Titapiwatanakun, V., Chutoprapat, R., 2020. Transfersomes: A Promising Nanoencapsulation Technique for Transdermal Drug Delivery. Pharmaceutics. 12, 1–23. https://doi.org/10.3390/PHARMACEUTICS12090855.

Oyarzún, P., Gallardo-Toledo, E., Morales, J., Arriagada, F., 2021. Transfersomes as alternative topical nanodosage forms for the treatment of skin disorders. Nanomedicine (Lond.) 16, 2465–2489. https://doi.org/10.2217/NNM-2021-0335.

Pcloquin, C.A., Namdar, R., Singleton, M.D., Nix, D.E., 1999. Pharmacokinetics of Rifampin Under Fasting Conditions, With Food, and With Antacids. Chest 115, 12–18. https://doi.org/10.1378/CHEST.115.1.12.

Peng, K., Vora, L.K., Tekko, I.A., Dian, A., Domínguez-, J., Ramadon, D., Chambers, P., Mccarthy, H.O., Larra, E., Donnelly, F., 2021. Dissolving microneedle patches loaded with amphotericin B microparticles for localised and sustained intradermal delivery: Potential for enhanced treatment of cutaneous fungal infections. J. Control. Release 339, 361–380. https://doi.org/10.1016/j.jconrel.2021.10.001.

Perlroth, J., Kuo, M., Tan, J., Bayer, A.S., Miller, L.G., 2008. Adjunctive use of rifampin for the treatment of Staphylococcus aureus infections: a systematic review of the literature. Arch. Intern. Med. 168, 805–819. https://doi.org/10.1001/ARCHINTE.168.8.805.

Permana, A.D., Mir, M., Utomo, E., Donnelly, R.F., 2020. Bacterially sensitive nanoparticle-based dissolving microneedles of doxycycline for enhanced treatment of bacterial biofilm skin infection: A proof of concept study. Int J Pharm X. 2, 100047 https://doi.org/10.1016/J.IJPX.2020.100047.

Pulido Pérez, A., Baniandrés Rodríguez, O., Ceballos Rodríguez, M.C., Mendoza Cembranos, M.D., Campos Domínguez, M., R., 2014. Suárez Fernández, Skin infections caused by community-acquired methicillin-resistant staphylococcus aureus: Clinical and microbiological characteristics of 11 cases. Actas Dermosifiliogr. 105, 150–158. https://doi.org/10.1016/j.adengl.2013.09.005.

Ranamukhaarachchi, S.A., Lehnert, S., Ranamukhaarachchi, S.L., Sprenger, L., Schneider, T., Mansoor, I., Rai, K., Häfeli, U.O., Stoeber, B., 2016. A micromechanical comparison of human and porcine skin before and after preservation by freezing for medical device development. Scientific Reports 6, 1–9. https://doi.org/10.1038/srep32074.

Rifampicin | Drugs | BNF | NICE, (n.d.). https://bnf.nice.org.uk/drugs/rifampicin/ (accessed April 27, 2023).

Rukavina, Z., Šegvić Klarić, M., Filipović-Grčić, J., Lovrić, J., Vanić, Ž., 2018. Azithromycin-loaded liposomes for enhanced topical treatment of methicillin-resistant Staphyloccocus aureus (MRSA) infections. Int. J. Pharm. 553, 109–119. https://doi.org/10.1016/J.IJPHARM.2018.10.024.

Sabri, A.H., Kim, Y., Marlow, M., Scurr, D.J., Segal, J., Banga, A.K., Kagan, L., Lee, J.B., 2020. Intradermal and transdermal drug delivery using microneedles – Fabrication, performance evaluation and application to lymphatic delivery. Adv. Drug Deliv. Rev. 153, 195–215. https://doi.org/10.1016/J.ADDR.2019.10.004.

Salwa, N.T., Chevala, S.R., Jitta, S.M., Marques, V.M., Vaz, L., 2021. Kumar, Polymeric microneedles for transdermal delivery of nanoparticles: Frontiers of formulation, sterility and stability aspects, J Drug Deliv. Sci. Technol. 65, 102711 https://doi.org/10.1016/J.JDDST.2021.102711.

Sartawi, Z., Blackshields, C., Faisal, W., 2022. Dissolving microneedles: Applications and growing therapeutic potential. J. Control. Release 348, 186–205. https://doi.org/10.1016/J.JCONREL.2022.05.045.

Shinde, U.A., Parmar, S.J., Easwaran, S., 2019. Metronidazole-loaded nanostructured lipid carriers to improve skin deposition and retention in the treatment of rosacea. Drug Dev. Ind. Pharm. 45, 1039–1051. https://doi.org/10.1080/03639045.2019.1569026.

Singh, C., Bhatt, T.D., Gill, M.S., Suresh, S., 2014. Novel rifampicin–phospholipid complex for tubercular therapy: Synthesis, physicochemical characterization and in-vivo evaluation. Int. J. Pharm. 460, 220–227. https://doi.org/10.1016/J.IJPHARM.2013.10.043.

Suaya, J.A., Eisenberg, D.F., Fang, C., Miller, L.G., 2013. Skin and Soft Tissue Infections and Associated Complications among Commercially Insured Patients Aged 0–64 Years with and without Diabetes in the U.S. PLoS One 8, e60057.

Sutradhar, I., Zaman, M.H., 2021. Evaluation of the effect of temperature on the stability and antimicrobial activity of rifampicin quinone. J. Pharm. Biomed. Anal. 197, 113941 https://doi.org/10.1016/J.JPBA.2021.113941.

Touitou, E., Meidan, V.M., Horwitz, E., 1998. Methods for quantitative determination of drug localized in the skin. J. Control. Release 56, 7–21. https://doi.org/10.1016/S0168-3659(98)00060-1.

Utomo, E., Domínguez-Robles, J., Moreno-Castellanos, N., Stewart, S.A., Picco, C.J., Anjani, Q.K., Simón, J.A., Peñuelas, I., Donnelly, R.F., Larrañeta, E., 2022. Development of intranasal implantable devices for schizophrenia treatment. Int. J. Pharm. 624, 122061 https://doi.org/10.1016/J.IJPHARM.2022.122061.

Versaevel, M., Grevesse, T., Gabriele, S., 2012. Spatial coordination between cell and nuclear shape within micropatterned endothelial cells. Nat. Commun. 3, 671. https://doi.org/10.1038/ncomms1668.

Wagner, A., Vorauer-Uhl, K., 2011. Liposome Technology for Industrial Purposes. J Drug Deliv. 2011, 1–9. https://doi.org/10.1155/2011/591325.

Wiedersberg, S., Guy, R.H., 2014. Transdermal drug delivery: 30 + years of war and still fighting! J. Control. Release 190, 150–156. https://doi.org/10.1016/J.JCONREL.2014.05.022.

Wu, H.L., Sheng, Y.J., Tsao, H.K., 2014. Phase behaviors and membrane properties of model liposomes: Temperature effect. J. Chem. Phys. 141 https://doi.org/10.1063/1.4896382/74936.

Yang, H., Wu, X., Zhou, Z., Chen, X., Kong, M., 2019. Enhanced transdermal lymphatic delivery of doxorubicin via hyaluronic acid based transfersomes/microneedle complex for tumor metastasis therapy. Int. J. Biol. Macromol. 125, 9–16. https://doi.org/10.1016/J.IJBIOMAC.2018.11.230.

Zasowski, E.J., Trinh, T.D., Claeys, K.C., Dryden, M., Shlyapnikov, S., Bassetti, M., Carnelutti, A., Khachatryan, N., Kurup, A., Pulido Cejudo, A., Melo, L., Cao, B., Rybak, M.J., 2022. International Validation of a Methicillin-Resistant Staphylococcus aureus Risk Assessment Tool for Skin and Soft Tissue Infections. Infect. Dis. Ther. 11, 2253–2263. https://doi.org/10.1007/S40121-022-00712-X.

Zheng, Z., Stewart, P.S., 2002. Penetration of Rifampin through Staphylococcus epidermidis Biofilms. Antimicrob. Agents Chemother. 46, 900. https://doi.org/10.1128/AAC.46.3.900-903.2002.

Zimmerli, W., Sendi, P., 2019. Role of Rifampin against Staphylococcal Biofilm Infections In Vitro, in Animal Models, and in Orthopedic-Device-Related Infections. Antimicrob. Agents Chemother. 63 https://doi.org/10.1128/AAC.01746-18.

Zoabi, A., Touitou, E., Margulis, K., 2021. Recent Advances in Nanomaterials for Dermal and Transdermal Applications. Colloids and Interfaces 5, 18. https://doi.org/10.3390/COLLOIDS5010018.